IOPscience iopscience.iop.org

Home Search Collections Journals About Contact us My IOPscience

Critical and multicritical semi-random (1 + *d*)-dimensional lattices and hard objects in *d* dimensions

This article has been downloaded from IOPscience. Please scroll down to see the full text article.

2002 J. Phys. A: Math. Gen. 35 897

(http://iopscience.iop.org/0305-4470/35/4/304)

View the table of contents for this issue, or go to the journal homepage for more

Download details:
IP Address: 171.66.16.109
The article was downloaded on 02/06/2010 at 10:32

Please note that terms and conditions apply.

INSTITUTE OF PHYSICS PUBLISHING JOURNAL OF PHYSICS A: MATHEMATICAL AND GENERAL

J. Phys. A: Math. Gen. **35** (2002) 897–927 PII: S0305-4470(02)24705-8

Critical and multicritical semi-random (1 + d)-dimensional lattices and hard objects in d dimensions

P Di Francesco and E Guitter

CEA-Saclay, Service de Physique Théorique, F-91191 Gif sur Yvette Cedex, France

E-mail: philippe@spht.saclay.cea.fr and guitter@spht.saclay.cea.fr

Received 8 May 2001
Published 18 January 2002
Online at stacks.iop.org/JPhysA/35/897

Abstract

We investigate models of (1 + d)D Lorentzian semi-random lattices with one random (space-like) direction and d regular (time-like) ones. We prove a general inversion formula expressing the partition function of these models as the inverse of that of hard objects in d dimensions. This allows for an exact solution of a variety of new models including critical and multicritical generalized (1 + 1)D Lorentzian surfaces, with fractal dimensions $d_F = k + 1$, $k = 1, 2, 3, \ldots$, as well as a new model of (1 + 2)D critical tetrahedral complexes, with fractal dimension $d_F = 12/5$. Critical exponents and universal scaling functions follow from this solution. We finally establish a general connection between (1+d)D Lorentzian lattices and directed-site lattice animals in (1 + d) dimensions.

PACS numbers: 05.50.+q, 02.10.Yn, 05.40.Fb

1. Introduction

The study of random lattices is an important subject relevant to many areas of physics such as quantum gravity or fluid membranes. One of the most efficient descriptions of such random lattices is through matrix models which generate discrete two-dimensional random surfaces in the form of tessellations made of tiles of arbitrary valences (for reviews see [1, 2] and references therein). The archetypical example is random triangulations perused in the context of 2D quantum gravity. Analogous tessellations can be considered in higher dimension but, unfortunately, no such powerful tool as matrix modelling is available, making the subject quite difficult. Recently a new type of random lattice was introduced [3] referred to as Lorentzian random lattices in which one particular (time) direction is regular while the other (space) ones are random. This allows us to view, for example, a (D + 1)-dimensional Lorentzian lattice as the time evolution of a D-dimensional usual random lattice. More generally, we may also

 © 2002 IOP Publishing Ltd Printed in the UK

consider semi-random lattices, with a number, say, D of random directions and d of regular ones. We shall refer to these lattices as $(D+d)$D Lorentzian lattices. These can be viewed as interpolations between regular lattices ($D = 0$) and fully random ones ($d = 0$). By a slight abuse of language, we shall refer to the d regular directions as 'time directions' and to the D random ones as 'space directions', although our analysis is purely statistical (no dynamics). The cases considered so far correspond to $d = 1$ and $D = 1$ [3,4] or 2 [5].

In this paper, we focus on the case of $D = 1$ and arbitrary $d \geqslant 1$, referred to as $(1+d)$D Lorentzian-type lattices in the following. For such models, we will derive a powerful *inversion relation*, expressing the partition function for such a $(1+d)$D Lorentzian lattice as the inverse of the partition function of some hard-object model on the time-like d-dimensional regular lattice. More precisely, this relation takes the general form

$$Z_{1+d}(\{t_i\}) = \frac{1}{Z_d^h(\{-t_i\})} \tag{1.1}$$

where $Z_{1+d}(\{t_i\})$ is the partition function of our $(1+d)$D Lorentzian lattices with activities t_i per tile of type i, and $Z_d^h(\{-t_i\})$ denotes the partition function of hard objects on the time-like d-dimensional regular lattice with activities $-t_i$ per hard object of corresponding type i. This relation (1.1) is very general, and holds for any dimension d and any *fixed* d-dimensional (but not necessarily regular) time lattice, any type of tile i, and even with time-dependent activities t_i. We may view the inversion relation (1.1) as some type of 'boson–fermion' correspondence, relating the partition function of weakly interacting bosons, namely the tiles of the lattice, to the inverse of that of locally interacting fermions, namely the hard objects with nearest neighbour exclusion.

As a first application, we show how to relate the partition function of $(1+1)$D Lorentzian triangulations to that of the hard-dimer model on a line, which allows for a very simple solution of the problem in terms of a 2×2 transfer matrix, as opposed to the previous solutions relying on transfer matrices of infinite size [3, 4, 6]. This new approach allows us to build and solve many more models of $(1+1)$D Lorentzian surfaces, such as those made of larger $(2(i+1)$-gonal) tiles, in connection with hard multimers on a line. In particular, we are able to reach new multicritical points for these surfaces, displaying new large scale universal properties, and fractal dimension $D_F = k+1$, $k = 1, 2, 3, \ldots$.

Going to a higher dimension, we then introduce a model of $(1+2)$D Lorentzian tetrahedral complexes, i.e. semi-random lattices made of tetrahedra, and apply our inversion relation to express its partition function in terms of that of 2D hard hexagons solved by Baxter [7]. As an outcome, we immediately obtain the large scale behaviour of these new semi-random lattices.

Analogous relations between $(1+d)$-dimensional problems and d-dimensional nearest-neighbour exclusion models have already been found in the context of directed-site lattice animal enumeration (DSAE) problems [8, 9]. This suggests the existence of a connection between Lorentzian-type $(1+d)$D Lorentzian lattices and $(1+d)$-dimensional DSAE. We will establish such a connection in which animals will appear as a particular subclass of Lorentzian lattices. Our inversion relation actually provides an alternative and more direct derivation of the equivalence between DSAE and nearest neighbour exclusion models.

The paper is organized as follows. In section 2, we discuss the case of Lorentzian $(1+1)$D surfaces. We initially derive the inversion formula by focusing on the simplest case of $(1+1)$D Lorentzian triangulations (section 2.1). This allows us to rederive, very simply, some of the known properties of these surfaces. In section 2.2, we extend the inversion formula to include $(1+1)$D Lorentzian surfaces made of time-like $2(i+1)$-gons with activity t_i $i = 1, 2, 3, \ldots$, now corresponding to hard $(i+1)$-mers on a line, and derive the corresponding thermodynamic

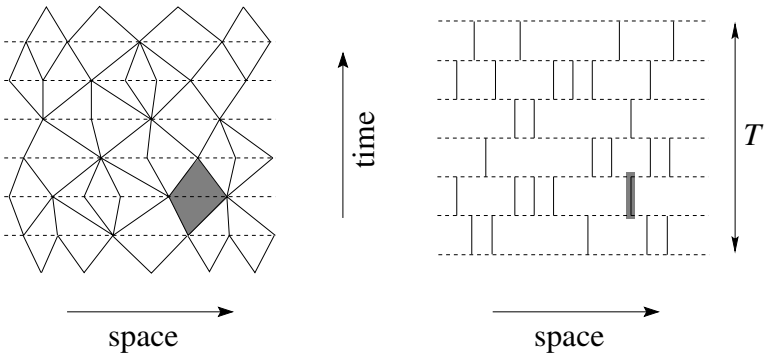

Figure 1. A typical (1 + 1)D Lorentzian triangulation together with its dual, made of T time slices. The triangulation is regular in the 'time' direction and random in the 'space' direction with an arbitrary succession of up and down triangles in each slice. Triangles of neighbouring slices may be paired so as to form time-like lozenges, such as the shaded one in the figure. These elementary building blocks translate into vertical edges in the dual picture.

partition function and loop–loop propagator. The first application concerns the case of surfaces made of only one type of such tiles (say $2(k+1)$-gons, with fixed k) and is discussed in section 2.3. Next we show in section 2.4 how to obtain multicritical models by fine-tuning the various activities t_i. For these models, we compute the corresponding scaling exponents as well as universal scaling functions. Section 3 is devoted to the study of (1 + 2)D Lorentzian tetrahedral complexes. We first define the model in section 3.1 in terms of plaquettes living in tubes of hexagonal section. We then apply in section 3.2 the inversion relation to obtain the critical behaviour of our model in terms of that of hard hexagons at the Lee–Yang edge singularity point. In section 4, we make the connection between our models and directed-site lattice animals, both in the (1 + 1)D case (section 4.1) and in the (1 + 2)D one (section 4.2). Finally, section 5 is devoted to a discussion of the (infinite) transfer matrices for our models. We first derive in section 5.1 the various (1+1)D transfer matrices in terms of the corresponding finite ones for hard objects on a line. The most technical cases of this discussion are treated in the appendix. We then use, in section 5.2, the equivalence to hard objects to construct more general parametric families of mutually commuting transfer matrices corresponding to integrable models containing our semi-random lattice models as particular points. We gather a few concluding remarks in section 6.

2. Critical and multicritical models of Lorentzian (1 + 1)D surfaces

2.1. Inversion principle: (1 + 1)*D Lorentzian triangulations versus 1D hard dimers*

In this section, we introduce the fundamental inversion formula relating the partition functions of Lorentzian-type semi-random lattices and hard objects in one less dimension. For simplicity, we specialize here to the simplest model of pure Lorentzian triangulations in (1 + 1)D, which corresponds to hard dimers on a line.

We start with the partition function $Z_T(t)$ of Lorentzian triangulations [3] with T time slices and an activity t per pair of neighbouring triangles sharing a space-like edge (see figure 1). The corresponding 'time-like' lozenges form the building blocks in the construction of the surfaces. In the dual picture, they translate into time-like (vertical) edges connecting successive space-like (horizontal) lines.

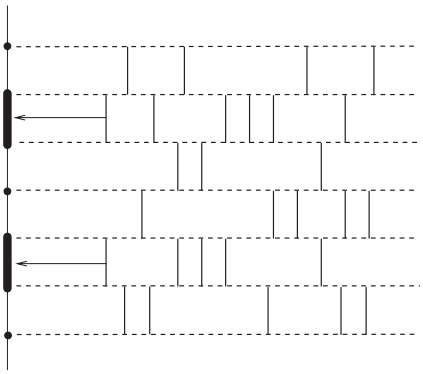

Figure 2. A configuration of (1 + 1)D Lorentzian triangulation in the dual picture, together with its left vertical projection. The latter is obtained by letting the foreground of the triangulation, made of the leftmost edges, slide horizontally all the way to the vertical line on the left. This projection clearly defines a hard-dimer configuration on the vertical line.

The idea behind the correspondence to hard dimers is to decompose the surface configurations according to their left vertical projection defined as follows. Let us allow for the vertical edges to slide along the horizontal direction without passing one-another, both within the same time slice and between two consecutive ones, thus preserving the relative positioning between them. We then single out those vertical edges which can be taken all the way to a vertical line on the left without moving the others. The resulting configuration of edges along this vertical line constitutes the left vertical projection of our surface. Clearly, it defines a hard-dimer configuration of the vertical integral segment $[0, T] \subset \mathbb{Z}$ as depicted in figure 2. To get dimers we simply view each edge as linking its two endpoints. The hardness simply means that any integer point in $[0, T]$ belongs to *at most* one dimer, translating into a mutual avoidance of dimers. This is due to the fact that on any two consecutive time slices, no more than one edge can be projected.

We therefore write the partition function $Z_T(t)$ as

$$Z_T(t) = \sum_{\text{hard dimer config. } C} t^{|C|}\, Z_T^{(C)}(t) \tag{2.1}$$

where the sum extends over all hard-dimer configurations C on the integer segment $[0, T]$ (including the empty one), and where $Z_T^{(C)}(t)$ is the restricted partition function involving those configurations having projection C, from which we have factored out the weight $t^{|C|}$ of the projected part, $|C|$ denoting the number of dimers in C. More generally we have the relations

$$t^{|D|} Z_T(t) = \sum_{C \supset D} t^{|C|}\, Z_T^{(C)}(t) \tag{2.2}$$

valid for any hard-dimer configuration D (equation (2.1) corresponding to $D = \emptyset$). This expresses the fact that by completing any configuration of Lorentzian triangulation with T time slices (in the dual picture) by a given left column of vertical edges (corresponding to a hard-dimer configuration D), one builds exactly once each configuration having a projection containing D, i.e. having D as a subconfiguration (see figure 3). This latter relation is easily inverted using the celebrated Möbius inversion[1] formula, leading to

$$t^{|C|}\, Z_T^{(C)}(t) = \sum_{D \supset C} (-1)^{|D|-|C|} t^{|D|} Z_T(t). \tag{2.3}$$

[1] Note that the Möbius inversion usually involves the opposite order relation $\subset$ but it works similarly for the order relation $\supset$ used here.

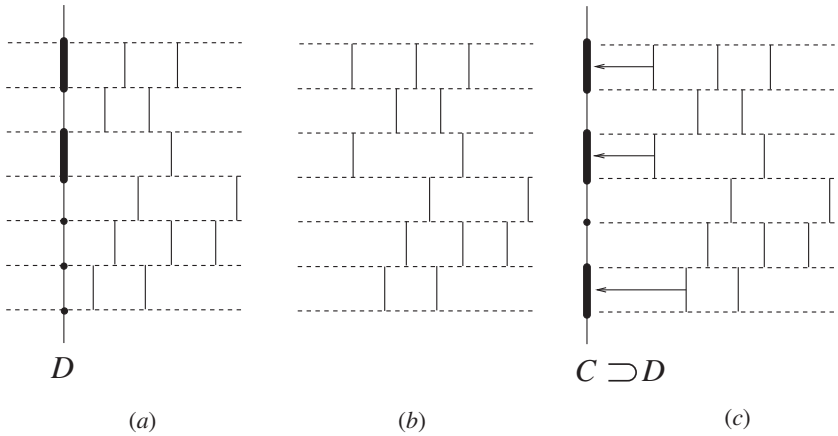

Figure 3. By completing an arbitrary Lorentzian triangulation with a hard-dimer configuration D (a), we build a larger triangulation (b) whose projection C contains D (c). With this procedure (with fixed D) we build, exactly once, all Lorentzian triangulations whose projection C contains D.

Noting that $Z_T(t)$ factors out of the sum on the rhs, we finally get

$$Z_T(t) = \frac{(-t)^{|C|}\, Z_T^{(C)}(t)}{\sum_{D\supset C}(-t)^{|D|}}. \tag{2.4}$$

Picking $C = \emptyset$, we arrive at our fundamental inversion relation

$$Z_T(t) = \frac{1}{Z_T^{hd}(-t)} \tag{2.5}$$

where

$$Z_T^{hd}(z) = \sum_{\text{hard dimer config. } D} z^{|D|} \tag{2.6}$$

denotes the standard partition function for hard dimers with fugacity z per dimer. As we already mentioned in the introduction, this relation is a generalization of the boson–fermion correspondence relating, for instance, the partition function $1/(1-t)$ of free bosons with fugacity t per particle on a point to the inverse of $1+z = 1-t$ of that of a fermion with fugacity $z = -t$ on a point.

Formula (2.4) also implies, upon substituting (2.6) that

$$Z_T^{(C)}(t) = \frac{Z_{[0,T]\setminus C}^{hd}(-t)}{Z_T^{hd}(-t)} \tag{2.7}$$

where

$$Z_{[0,T]\setminus C}^{hd}(z) = \sum_{D\supset C} (z)^{|D|-|C|} \tag{2.8}$$

is the hard-dimer partition function on the segment $[0, T]$ minus the occupied points of C.

The above construction is very general. In particular, our inversion formula (2.5) also holds if we attach an extra fugacity w_s per edge inside the time slice s resulting in a total weight $z_s = -t\,w_s$ per dimer in the slice s in the hard-dimer language, allowing in particular to recover the loop–loop propagator (partition function with a fixed number of triangles at times 0 and T), and correlation functions for the numbers of triangles in given slices. It will also be extended in

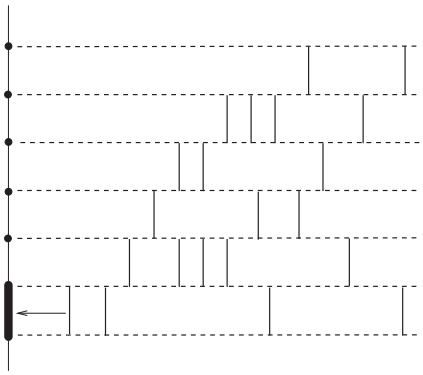

Figure 4. A typical Lorentzian triangulation with projection C_0, made of a single dimer in the lowest position. This induces a staircase-type boundary condition on the left side of the triangulation, namely that any edge in a given time slice must have at least one edge on its left in the slice just below.

section 2.2 below to the case of surfaces made of larger building blocks corresponding to hard multimers on a line. Finally in section 3 we will extend it to higher-dimensional semi-random lattices.

With this construction we have reduced the (1 + 1)D Lorentzian gravity-type problems to that, much simpler, of hard objects on a line.

To complete this section, let us re-derive the partition function of pure Lorentzian triangulations $Z_T(t)$ from the hard-dimer equivalence. The partition function $Z_T^{hd}(z)$ is easily computed by use of a 2×2 transfer matrix $\mathcal{T}$ between successive segments in either empty or occupied states:

$$Z_T^{hd}(z) = v^t \mathcal{T}^{T+1} v = (\,1 \quad 0\,) \begin{pmatrix} 1 & 1 \\ z & 0 \end{pmatrix}^{T+1} \begin{pmatrix} 1 \\ 0 \end{pmatrix}. \tag{2.9}$$

We may read directly from this the asymptotic large T behaviour of $Z_T(t)$. Indeed, (2.9) is dominated for large T by the largest eigenvalue λ_+ of $\mathcal{T}$, satisfying $\lambda^2 - \lambda - z = 0$ (with solutions $\lambda_\pm(z) = (1 \pm \sqrt{1+4z})/2$). Therefore we find that for large T

$$Z_T(t) = \frac{1}{Z_T^{hd}(-t)} \sim \mu^T(t) \qquad \text{where} \quad \mu(t) = \frac{1}{\lambda_+(-t)} \tag{2.10}$$

is the *smallest* solution of

$$\mu = 1 + t\mu^2 \tag{2.11}$$

namely the celebrated generating function of the Catalan numbers $\mu(t) = (1-\sqrt{1-4t})/(2t)$. More precisely, we have

$$Z_T^{hd}(z) = \frac{\lambda_+(z)^{T+2} - \lambda_-(z)^{T+2}}{\lambda_+(z) - \lambda_-(z)} \tag{2.12}$$

leading to

$$Z_T(t) = \frac{1-q^2}{1+q^2} \frac{(1+q^2)^{T+2}}{1-q^{2(T+2)}} \tag{2.13}$$

where we have set $q = \sqrt{t}\mu(t)$ (or equivalently $1/\sqrt{t} = q + 1/q$). Expanding the denominator in (2.13) we immediately read the eigenvalues of the infinite transfer matrix

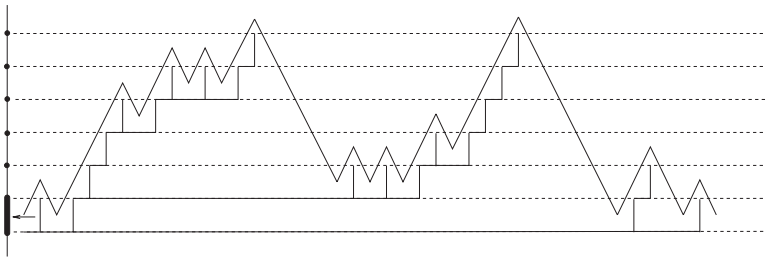

Figure 5. The one-to-one correspondence between 'left staircase boundary' triangulations and random walks from the origin to itself on the integer half-line. We first rewrite the configuration of edges forming the triangulation as a tree, by connecting each edge to that sitting just below on its left (connections are represented by thick horizontal lines here). By following the contour of the tree from the lower left branch to the lower right, the sequence of ascents and descents gives rise to the directed walk represented in the thin solid line (to get a nice directed walk, we must first place each vertical edge at a horizontal position equal to the total number of ascents and descents along the tree preceding it). Conversely, each such walk gives rise to a unique tree, therefore to a unique triangulation with the staircase boundary condition. This correspondence includes the empty triangulation with projection $\emptyset$, corresponding to the walk of 0 step.

for Lorentzian triangulations $(q+\frac{1}{q})q^{2n+1}$, $n=0,1,2,\ldots$, thus recovering the harmonic oscillator eigenvalues [4, 6].

As a final remark, we may interpret $\mu(t)$ as the partition function of a subclass of triangulations on the semi-infinite time interval $[0,\infty)$. To get a finite partition function it is sufficient to demand that the projection of the configurations is either the vacuum or the hard-dimer configuration C_0 made of a single dimer in the first slice (at time 0, see figure 4). This implies a so-called 'staircase' boundary condition on the left of the configurations, namely that an edge occurs in the slice s only if an edge already occurred on its left in the slice $s-1$ below. Indeed, we write this partition function as

$$1+t\lim_{T\to\infty} Z_T^{(C_0)}(t) = 1+t\lim_{T\to\infty}\frac{Z^{hd}_{[0,T]\setminus C_0}(-t)}{Z^{hd}_{[0,T]}(-t)} = 1+t\lim_{T\to\infty}\frac{\mu^T}{\mu^{T-2}} = 1+t\mu^2=\mu. \tag{2.14}$$

As explained in [4] and depicted in figure 5, the configurations above are in one-to-one correspondence with discrete random walks with steps of ± 1 on the integral half-line $[0,\infty)$, starting and ending at the origin, and with a weight t per ascending step.

As we will see in the following sections, all the presented equivalences will nicely generalize to more involved cases.

2.2. Generalized $(1+1)$*D Lorentzian surfaces versus 1D hard multimers*

In this section, we introduce generalized discrete Lorentzian surfaces consisting of various tiles, including lozenges, hexagons, octagons, etc. To be more precise, we wish to compute the partition function $Z_T(\{t_i\})$ of surfaces which in the dual picture look like figure 6, with vertical edges of arbitrary length with a fugacity t_i per edge of total length i, $i=1,2,3\ldots$ and taken on a time segment $[0,T]$. These edges are dual to particular time-like $2(i+1)$-gons (see figure 6(a)). The inversion formula (2.5) generalizes straightforwardly to this case. Firstly we now have the generalization of equation (2.2)

$$\prod_i t_i^{n_i(D)} Z_T(\{t_i\}) = \sum_{C\supset D}\prod_i t_i^{n_i(C)}\, Z_T^{(C)}(\{t_i\}) \tag{2.15}$$

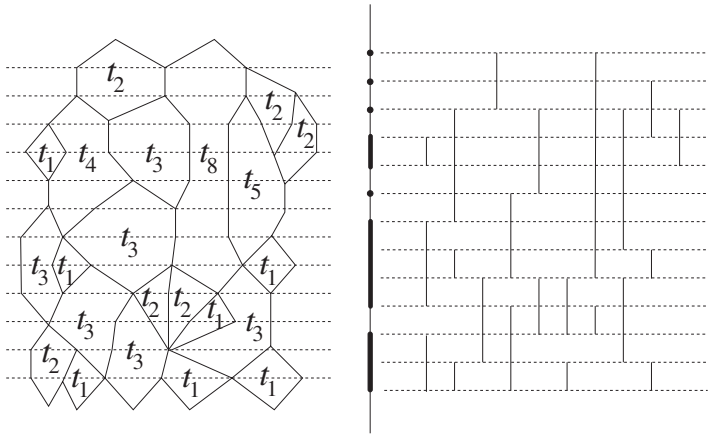

Figure 6. A typical generalized (1+1)D discrete Lorentzian surface (a) made of time-like lozenges, hexagons, octagons, etc respectively weighted by $t_1, t_2, t_3, \ldots$. Its dual (b) is made of vertical edges of length $1, 2, 3, \ldots$. extending over several time slices. The corresponding left vertical projection is nothing but a configuration of the hard-multimer model on the integer segment $[0, T]$.

where D (resp. C) denote hard-multimer configurations on the integral segment $[0, T]$ with $n_i(D)$ (resp. $n_i(C)$) $(i+1)$-mers. Again in such a configuration hard multimers avoid one-another in that a given point may belong to at most one multimer. By inclusion of configurations $C \supset D$ we mean that C contains all the multimers of D plus, possibly, others. Equations (2.15) are easily inverted by the Möbius inversion formula to finally yield

$$Z_T(\{t_i\}) = \frac{1}{Z_T^{hm}(\{z_i = -t_i\})} \tag{2.16}$$

where $Z_T^{hm}(\{z_i\})$ denotes the partition function of hard multimers on the integral segment $[0, T]$ with a fugacity z_i per $(i+1)$-mer.

Again, in the hard-multimer language we simply have to diagonalize the corresponding transfer matrix. Let us fix for definiteness a maximal length k for the edges, corresponding to a model of di-, tri-, $\ldots$, $(k+1)$-mers. This truncates the transfer matrix to a size $(k+1) \times (k+1)$, where the $(k+1)$ possible states correspond to the empty state, the state occupied by the lowest monomer of a $(i \geqslant 1)$-mer, the state occupied by the second lowest monomer of a $(i \geqslant 2)$-mer. The transfer matrix then reads

$$\mathcal{T}_k = \begin{pmatrix} 1 & 1 & 1 & \cdots & 1 & 1 \\ z_1 & 0 & 0 & \cdots & 0 & 0 \\ 0 & \frac{z_2}{z_1} & 0 & \cdots & 0 & 0 \\ 0 & 0 & \frac{z_3}{z_2} & \cdots & 0 & 0 \\ \vdots & \vdots & \ddots & \ddots & \ddots & \vdots \\ 0 & 0 & \cdots & \cdots & \frac{z_k}{z_{k-1}} & 0 \end{pmatrix} \tag{2.17}$$

and the partition function is expressed as

$$Z_T^{hm}(\{z_i\}) = v^t \left(\mathcal{T}_k\right)^{T+1} v \tag{2.18}$$

where $v^t = (1, 0, 0, \ldots, 0)$. Again the large T asymptotics of (2.16) are governed by the largest eigenvalue $\lambda(\{z_i\})$ of $\mathcal{T}_k$, leading to

$$Z_T(\{t_i\}) \sim \mu^T(\{t_i\}) \tag{2.19}$$

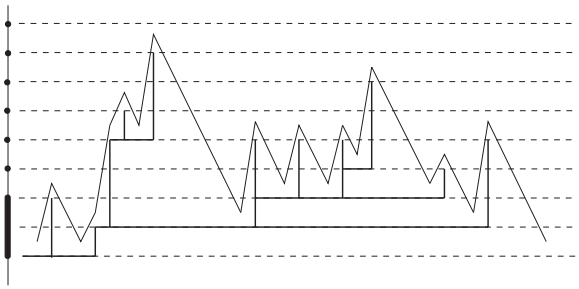

Figure 7. The one-to-one correspondence between 'left staircase boundary' generalized discrete Lorentzian surfaces and random walks from the origin to itself on the integer half-line, with ascending steps of arbitrary length and descending steps of -1. As in the triangulation case, we associate to each 'left staircase boundary' surface configuration a tree connecting each edge to that sitting just below it on its left. The walk is then defined as a walk along the tree, with the convention that it makes an ascending step of $+i$ when going up along an $(i+1)$-mer, whereas it only makes descending steps of -1 (again to best represent it as a directed walk, we must place the edges at horizontal positions equal to the total number of ascents and descents preceding them). Conversely any such walk gives rise to a unique tree with branches of arbitrary integer lengths and therefore a unique 'left staircase boundary' surface.

where $\mu(\{t_i\}) = 1/\lambda(\{z_i = -t_i\})$ is the smallest (in module) solution of the characteristic equation

$$\mu = 1 + \sum_{i=1}^{k} t_i \mu^{i+1} \tag{2.20}$$

Here again, μ may be interpreted as the partition function for the particular Lorentzian surfaces with semi-infinite time interval $[0, \infty)$, having a projection either empty (contribution of 1 in the rhs of (2.20)), or equal to a single multimer of either length i, extending over the i first time slices, $i = 1, 2, \ldots, k$ (contributions of $t_i \mu^{i+1}$ in the rhs of (2.20)).

As before, these configurations are in one-to-one correspondence with discrete random walks from 0 to 0 on the integral half-line $[0, \infty)$, with possible ascending steps of $+i$, $i = 1, 2, \ldots, k$, weighted by t_i, and descending steps -1 (see figure 7). The partition function μ of these walks clearly satisfies the self-consistent equation (2.20) corresponding to a decomposition of the walks according to the length i of their first ascending step, with μ^{i+1} being the partition function of the rest of the walk going from position i back to the origin on the half-line.

Another quantity of interest is the so-called loop–loop propagator $Z_T(i, j|\{t_m\})$ defined as the partition function of surfaces with T time slices and with fixed numbers i (resp. j) of tiles originating (resp. terminating) in the first (resp. last) slice. The inversion formula (2.16) extends straightforwardly to include an extra weight w_s attached to each portion of tile visiting the slice $s = 0, 1, \ldots, T$. Choosing $w_0 = x$, $w_T = y$ and $w_s = 1$ for $s = 1, 2, \ldots, T-1$, we immediately get the generating function $G_T(x, y|\{t_m\}) = \sum_{i,j \geqslant 0} x^i y^j Z_T(i, j|\{t_m\})$ as the inverse of the partition function $G_T^{hm}(x, y|\{z_m\})$ of hard multimers with weights $z_m = -t_m$ for $(m+1)$-mers and extra weights x (resp. y) for the multimers originating (resp. terminating) at point 0 (resp. T). To compute $G_T^{hm}(x, y|\{z_m\})$ we make the simple observation that it is at most linear in the variables x and y as at most one multimer can touch the point 0 (resp. T), and that it is symmetric in x and y. Writing

$$G_T^{hm}(x, y|\{z_m\}) = a - b(x+y) + cxy \tag{2.21}$$

we easily compute the coefficients a, b, c by taking particular values of x and y. For $x = y = 0$, we forbid multimers to touch the extremities of the segment $[0, T]$ thus effectively reducing it to $[1, T-1]$ and resulting in $a = Z^{hm}_{T-2}(\{z_m\})$. For $x = 1$ and $y = 0$ we only forbid the T point, with the result $a - b = Z^{hm}_{T-1}(\{z_m\})$. Finally, for $x = y = 1$ we simply have $a - 2b + c = Z^{hm}_{T}(\{z_m\})$. This results in the following expression for the loop–loop propagator

$$G_T(x, y|\{t_m\}) = \frac{1}{Z^{hm}_{T-2} - (x+y)(Z^{hm}_{T-2} - Z^{hm}_{T-1}) + xy(Z^{hm}_{T-2} - 2Z^{hm}_{T-1} + Z^{hm}_{T})} \tag{2.22}$$

where the Z^{hm}_N are all taken at the values $z_m = -t_m$. Explicitly expanding this as a series in x and y, we obtain

$$Z_T(i, j|\{t_m\}) = \frac{1}{Z^{hm}_{T-2}} \left(1 - \frac{Z^{hm}_{T-1}}{Z^{hm}_{T-2}}\right)^{i+j} \sum_{r \geqslant 0} \binom{i}{r}\binom{j}{r} \left(\frac{(Z^{hm}_{T-1})^2 - Z^{hm}_{T} Z^{hm}_{T-2}}{(Z^{hm}_{T-2} - Z^{hm}_{T-1})^2}\right)^r. \tag{2.23}$$

2.3. First application: hard $(k+1)$-mers and Fuss–Catalan numbers

As a first simple application of our construction, let us consider surfaces made only of time-like $2(k+1)$-gons, i.e. with duals made only of vertical edges of fixed length k. This corresponds to specializing to $t_i = \delta_{i,k} t$, where t is the weight per tile. In the limit of large T, this yields the thermodynamic partition function $Z^{(k)}_T(t) \sim \mu^T(t)$ where $\mu(t)$ is the smallest solution (in module) of $t\mu^{k+1} = \mu - 1$, known as the generating function of the Fuss–Catalan numbers $c^{(k)}_n$ [10]

$$\mu(t) = \sum_{n \geqslant 0} c^{(k)}_n t^n \qquad \text{where} \quad c^{(k)}_n = \frac{((k+1)n)!}{(kn+1)!n!}. \tag{2.24}$$

From the use of Stirling's formula, we get the large n behaviour of these numbers: $c^{(k)}_n \sim \left((k+1)^{k+1}/k^k\right)^n / n^{3/2}$, which allows us to show that for all $k \geqslant 1$, the function $\mu(t)$ displays a square root singularity $\mu|_{\text{sing}} \sim \sqrt{t_c - t}$ when t approaches the critical value

$$t_c = \frac{k^k}{(k+1)^{k+1}}. \tag{2.25}$$

Therefore the scaling limit of these models (for all $k \geqslant 1$) lies in the same universality class as that of pure Lorentzian triangulations, corresponding to $k = 1$.

Note finally that according to the above equivalence with random walks, the function $\mu(t)$ also generates the numbers of directed random walks on the integer half-line $[0, \infty)$ starting and ending at 0 and with ascending steps of $+k$ only and descending steps of -1, and with a weight t per ascending step.

2.4. Second application: multicritical models of $(1+1)$D Lorentzian surfaces and Patalan numbers

In this section we show how to go beyond the generic square root singularity of pure Lorentzian surfaces and obtain more interesting critical behaviours. As usual, this can be achieved by fine-tuning the weights t_i in order to reach multicritical points. Indeed, we may reach a multicritical point of order $(k+1)$ by retaining di-, tri-, ..., $(k+1)$-mers and fine-tuning the activities t_i, $i = 1, 2, \ldots, k$ in order for equation (2.20) to take the form

$$\left(1 - \frac{2}{k} t\mu\right)^{k+1} = 1 - \frac{2(k+1)}{k} t \tag{2.26}$$

namely by picking

$$t_i = -\frac{1}{k+1}\binom{k+1}{i+1}\left(-\frac{2t}{k}\right)^i \qquad i = 1, 2, \ldots, k \tag{2.27}$$

all expressed in terms of the activity $t = t_1$ per lozenge. The values of the coefficients in (2.26) are entirely fixed by the constant, linear and quadratic terms in (2.20), with relative values 1, -1 and t. This yields the thermodynamic partition function per time slice

$$\mu(t) = \frac{k}{2t}\left(1 - \left(1 - \frac{2(k+1)}{k}t\right)^{\frac{1}{k+1}}\right). \tag{2.28}$$

For instance, for $k = 2$, we reach a tricritical point by taking activities t per lozenge and $-t^2/3$ per hexagon, leading to $\mu = (1 - (1 - 3t)^{\frac{1}{3}})/t$. The need for both positive and negative activities to reach a multicritical point parallels the case of ordinary random surfaces as solved by means of the one-matrix models, whose potentials display the same pattern of alternating signs for the activities per tiles. Also note that, as in that case, we need to consider *at least* $(k+1)$-mers to reach a multicritical point of order $(k+1)$. In that respect, equation (2.26) is the minimal realization of the $(k+1)$-critical point in which the requirement of multicriticality fixes all the t_i in terms of $t = t_1$. The same point could be attained from any model also involving larger multimers leading to a characteristic equation of degree larger than $k+1$. The corresponding $(k+1)$-critical point then involves $k-1$ relations between $t_1, t_2, \ldots, t_k, \ldots$.

Up to the change of variables $t = k(k+1)x/2$, the function $\mu = \sum_{n\geqslant 0} p_n^{(k)} x^n$ (2.28) is known as the generating function of so-called Patalan numbers [11]

$$p_n^{(k)} = \frac{(k+1)^n}{(n+1)!}\prod_{i=1}^{n}((k+1)i - 1) \tag{2.29}$$

which are all positive integers. The integrality of these numbers is clear from equation (2.27), since all the t_i are integer multiples of x^i. On the other hand, the positivity appears as non-trivial, as the t_i have alternating signs. This strongly suggests a possible purely combinatorial reinterpretation of our multicritical partition functions.

The singularity of (2.28) leads to a new scaling behaviour for the corresponding decorated surfaces, when t approaches the multicritical point $t_c = k/(2(k+1))$. Indeed, to get a proper scaling limit of the multicritical partition function $Z_T^{[k]}(t) = Z_T(\{t_i\}) \sim \mu^T$, corresponding to the fine-tuning (2.27) and with μ as in (2.28), we must set

$$T = \frac{\tau}{a} \qquad t = t_c(1 - a^{k+1}\Lambda) \tag{2.30}$$

where τ is the renormalized time lapse and where Λ is the renormalized activity per unit area of tile ('cosmological constant'), with $a \to 0$ in the scaling regime. In this regime, $(\mu(t)/\mu(t_c))^T \to \mathrm{e}^{-\tau\Lambda^{\frac{1}{k+1}}}$ and more generally $Z_T^{[k]}(t)/Z_T^{[k]}(t_c)$ becomes a universal scaling function of $\tau\Lambda^{\frac{1}{k+1}}$ which we will determine[2]. Introducing the area $A = \sum_{i\geqslant 1} i N_i$ where N_i is the total number of $2(i+1)$-gonal tiles forming the surface, we see that the total Boltzmann weight is proportional to t^A. Writing $t^A \sim t_c^A \mathrm{e}^{-A\frac{t_c - t}{t_c}}$ when $t \to t_c$, and substituting (2.30), we see that the parameter Λ is conjugate to the renormalized area of the surface, defined as $\mathcal{A} = a^{k+1}A$. We immediately deduce that $\mathcal{A} \sim \tau^{k+1}$ and get the scaling behaviour of the area of the surface

$$A \sim T^{k+1} \tag{2.31}$$

[2] Note that this scaling function involves μ as well as the other roots of the polynomial equation (2.26) as they all merge at the multicritical point.

in terms of the time lapse T when T is large. This determines the 'fractal dimension of space–time' to be $d_F = k+1$. In the directed random walk picture of the previous section, this allows us to obtain the scaling behaviour of the vertical extent or gyration radius $R = T$ of the walks on $[0, \infty)$, in terms of their total length $L = 2A$, namely $R \sim L^{\nu}$ with the exponent

$$\nu = \frac{1}{d_F} = \frac{1}{k+1}. \tag{2.32}$$

This is also the exponent of the correlation length $\xi \sim (t_c - t)^{-\nu}$ appearing, for instance, in the correlation of the numbers of tiles $\mathcal{N}(T_1), \mathcal{N}(T_2)$ in two given time slices at times T_1, T_2, namely $\langle \mathcal{N}(T_1)\mathcal{N}(T_2)\rangle \sim \mathrm{e}^{-\frac{|T_1-T_2|}{\xi}}$. The partition function of the walks of fixed length L is identified with the coefficient of $t^{\frac{L}{2}}$ in the expansion of $\mu(t)$ (2.28), and behaves as $(t_c)^{-\frac{L}{2}} L^{\alpha-3}$ with the susceptibility exponent

$$\alpha = \frac{2k+1}{k+1}. \tag{2.33}$$

Equivalently, in the language of random surfaces, the coefficient of t^A in the expansion of $\mu(t)$ (2.28) represents the thermodynamic partition function Z_A of fine-tuned semi-random surfaces of fixed area A and with fixed projection either empty or reduced to a single multimer. Therefore the exponent α (2.33) is interpreted as a configuration exponent for these objects, namely $Z_A \sim (t_c)^{-A} A^{\alpha-3}$ for large A. Note finally that, as expected, the exponents α and ν obey the hyperscaling relation $2 - \alpha = d\nu$ in $d = 1$ dimension.

To conclude this section, let us derive the explicit form of the finite-time partition function $Z_T^{[k]}(t)$ for the fine-tuned semi-random surfaces and its scaling limit, together with that of the corresponding loop–loop propagator. Starting from the inversion formula (2.16), we are left with the calculation of the partition function of fine-tuned hard multimers $Z_T^{hm[k]}$ expressed as

$$Z_T^{hm[k]} = v^t \left(\mathcal{T}_k\right)^{T+1} v \tag{2.34}$$

where the $(k+1) \times (k+1)$ transfer matrix reads as in (2.17) with $z_i = -t_i$ given by (2.27), and where $v^t = (1, 0, 0, \ldots, 0)$. The eigenvalues λ_j, $j = 0, 1, \ldots, k$ of this transfer matrix are simply the inverses of the solutions μ_j to the multicritical characteristic equation (2.26), reading

$$\mu_j = \frac{k}{2t}(1 - \omega^j \Delta) \qquad \text{with} \quad \omega = \mathrm{e}^{2\mathrm{i}\frac{\pi}{k+1}} \qquad \Delta = \left(1 - \frac{2(k+1)}{k} t\right)^{\frac{1}{k+1}}. \tag{2.35}$$

The partition function (2.34) is expressed as a linear combination $Z_T^{hm[k]} = \sum_{0 \leqslant j \leqslant k} a_j/(\mu_j)^{T+1}$, where the coefficients a_j may be obtained by explicit diagonalization of $\mathcal{T}_k$. After some algebra we find the rather simple expression

$$Z_T^{hm[k]} = \frac{1}{\Delta^k} \left(\frac{2t}{k}\right)^{T+2} \sum_{j=0}^{k} \frac{\omega^j}{(1 - \omega^j \Delta)^{T+2}} \tag{2.36}$$

which reduces to (2.12) for $k = 1$. Note that it satisfies the recursion relation $Z_{T+1}^{hm[k]} = Z_T^{hm[k]} - \sum_{i=1}^{k} t_i Z_{T-i}^{hm[k]}$ with the fine-tuned values of t_i (2.27). The solution (2.36) is the unique function obeying this recursion relation with the initial conditions: $Z_{-i}^{hm[k]} = 0$, $i = 2, 3, \ldots, k+1$ and $Z_{-1}^{hm[k]} = 1$. For illustration, let us display the first few values of $Z_T^{hm[k]}$ for non-negative T:

$$\begin{aligned} Z_0^{hm[k]} &= 1 \\ Z_1^{hm[k]} &= 1 - t \\ Z_2^{hm[k]} &= 1 - 2t + \frac{2(k-1)}{3k} t^2 \\ Z_3^{hm[k]} &= 1 - 3t + \frac{7k-4}{3k} t^2 - \frac{(k-1)(k-2)}{3k^2} t^3. \end{aligned} \tag{2.37}$$

By use of the inversion formula (2.16), the expression (2.36) finally leads to the partition function of multicritical semi-random surfaces

$$Z_T^{[k]}(t) = \left(\frac{k}{2t}\right)^{T+2} \frac{\Delta^k}{\sum_{j=0}^{k} \frac{\omega^j}{(1-\omega^j\Delta)^{T+2}}}. \tag{2.38}$$

Note that as $t \to t_c = k/(2(k+1))$, $\Delta \to 0$, the partition function (2.38) tends to a finite limit, as the denominator is of order Δ^k. This yields a finite ratio

$$\frac{Z_T^{[k]}(t)}{Z_T^{[k]}(t_c)} = (k+1)\left(\frac{t_c}{t}\right)^{T+2} \binom{T+1+k}{k} \frac{\Delta^k}{\sum_{j=0}^{k} \frac{\omega^j}{(1-\omega^j\Delta)^{T+2}}}. \tag{2.39}$$

We may now perform the scaling limit (2.30) of this ratio, that tends to a universal scaling function of the variable $x = \tau \Lambda^{\frac{1}{k+1}}$, namely

$$\lim_{a\to 0} \frac{Z_T^{[k]}(t)}{Z_T^{[k]}(t_c)} = \frac{k+1}{k!} \frac{x^k}{h_1(x)} \qquad x = \tau \Lambda^{\frac{1}{k+1}} \tag{2.40}$$

where we have used the generalized hyperbolic function h_1 of order $k+1$, a member of the family $h_p(x)$, $p = 1, 2, \ldots$, defined by

$$h_p(x) = \sum_{j=0}^{k} \omega^{pj} \mathrm{e}^{\omega^j x} \tag{2.41}$$

with ω as in (2.35). The functions h_p are cousins of the Mittag–Leffler function [12], generalizing the hyperbolic sine and cosine (case $k = 1$, $p = 1, 2$, respectively). Indeed for $k = 1$, with $h_1(x) = 2\sinh(x)$, (2.40) allows us to recover the usual scaling function $x/\sinh(x)$ [4].

We can fix the normalization of the partition function in order for its scaling limit to read

$$\mathcal{Z}_\tau^{[k]}(\Lambda) \equiv \frac{1}{(k+1)!} \lim_{a\to 0} \frac{Z_T^{[k]}(t)}{(k+1)^T} = \frac{(k+1)\Lambda^{\frac{k}{k+1}}}{k! h_1(\tau \Lambda^{\frac{1}{k+1}})} \tag{2.42}$$

and accordingly the critical value $\mathcal{Z}_\tau^{[k]}(0) = 1/\tau^k$. In particular, this allows us to recover, for $k = 1$, the partition function $\mathcal{Z}_\tau^{[1]}(\Lambda) = \sqrt{\Lambda}/\sinh(\tau\sqrt{\Lambda})$ of [4].

Let us now turn to the loop–loop propagator (2.23). To define a sensible scaling limit of this quantity we need to take

$$i = \frac{L_1}{a} \qquad j = \frac{L_2}{a} \tag{2.43}$$

and to substitute in (2.23) the value of the hard-multimer partition function

$$Z_{T-2}^{hm} \propto \frac{1}{(k+1)^T} h_1(\tau \Lambda^{\frac{1}{k+1}}) \tag{2.44}$$

with h_1 as in (2.41). Indeed, except for the prefactor $1/Z_{T-2}^{hm}$ which we normalize as in (2.42), only ratios of Z_T^{hm} enter the expression (2.23) so we may forget about all the prefactors

independent of T as indicated in (2.44) by the proportionality symbol. Equation (2.23) finally takes the scaling form

$$G_\tau^{[k]}(L_1, L_2) = \mathcal{Z}_\tau^{[k]}(\Lambda)\ \exp\left(-(L_1+L_2)\frac{\Lambda^{\frac{1}{k+1}}}{k}\frac{h_2}{h_1}\right) I_0\left(2\sqrt{L_1L_2\frac{\Lambda^{\frac{2}{k+1}}}{k^2}\frac{h_2^2-h_1h_3}{h_1^2}}\right) \quad (2.45)$$

with $\mathcal{Z}_\tau^{[k]}(\Lambda)$ as in (2.42), with $I_0(2x) = \sum_{r\geqslant 0} x^{2r}/(r!)^2$ the modified Bessel function, and where the hyperbolic functions $h_p \equiv h_p(\tau\Lambda^{\frac{1}{k+1}})$ are defined in (2.41). For completeness, let us display the hyperbolic functions entering the loop–loop propagator for the first few values of $k = 1, 2, 3$.

$$\begin{aligned}
&k=1: h_1(x) = h_3(x) = 2\sinh(x) \qquad h_2(x) = 2\cosh(x)\\
&k=2: h_m(x) = \mathrm{e}^{x} + 2\mathrm{e}^{-\frac{x}{2}}\cos\left(\frac{\sqrt{3}}{2}x + 2m\frac{\pi}{3}\right) \qquad m=1,2,3\\
&k=3: h_1(x) = 2(\sinh(x)-\sin(x)) \qquad h_2(x) = 2(\cosh(x)-\cos(x))\\
&h_3(x) = 2(\sinh(x)+\sin(x)).
\end{aligned} \quad (2.46)$$

With these, we recover in the $k = 1$ case the results of [4].

Let us finally comment on the form of the rescaled partition function $\mathcal{Z}_\tau^{[k]}(\Lambda)$ (2.42). In terms of the rescaled variable $x = \tau\Lambda^{\frac{1}{k+1}}$, it has poles situated at the complex non-vanishing zeros of $h_1(x)$, all of the form $x_{j,m} = -\omega^j\alpha_m^{\frac{1}{k+1}}$, $j = 0, 1, 2, \ldots, k$ and $m = 1, 2, 3, \ldots$ with α_m real positive. This allows us to write the partition function as

$$\mathcal{Z}_\tau^{[k]}(\Lambda) = \frac{1}{\tau^{k+1}\prod_{m=1}^{\infty}(1+\frac{\Lambda\tau^{k+1}}{\alpha_m})}. \quad (2.47)$$

When $k = 1$ we simply have $\alpha_m = \pi^2m^2$, $m = 1, 2, 3\ldots$. For arbitrary k there is no such simple form, but asymptotically one can show that

$$\alpha_m = \frac{\pi^{k+1}}{\sin^{k+1}(\frac{\pi}{k+1})}\left(m + \frac{k-1}{2(k+1)} + \mathrm{O}(\mathrm{e}^{-\epsilon m})\right)^{k+1}. \quad (2.48)$$

3. (1 + 2)D Lorentzian tetrahedral complexes and the hard-hexagon model

In this section, we consider three-dimensional random objects made of tetrahedra, corresponding to (1 + 2)D Lorentzian tetrahedral complexes, with two (time-like) regular directions and one (space-like) random one. This is in contrast with the more complicated situation of discrete (2 + 1)D Lorentzian manifolds used in the context of 3D gravity [5], which have one (time-like) regular direction and two (space-like) random ones. Still, by slightly breaking the symmetry in the two time directions, we shall be able to view the configurations of our model as the time evolution of some particular random triangulations, namely the Lorentzian ones.

3.1. The plaquette model for Lorentzian tetrahedral complexes

If we view the pure (1 + 1)D Lorentzian triangulations in the dual picture as a regular array of slices in which edges may freely slide horizontally provided they do not cross one-another, a natural (1 + 2)D generalization consists in having a regular 2D array of horizontal tubes in which plaquettes may freely slide horizontally, provided they do not cross one-another. More precisely, we consider here the situation depicted in figure 8(*a*), where the tubes have a regular

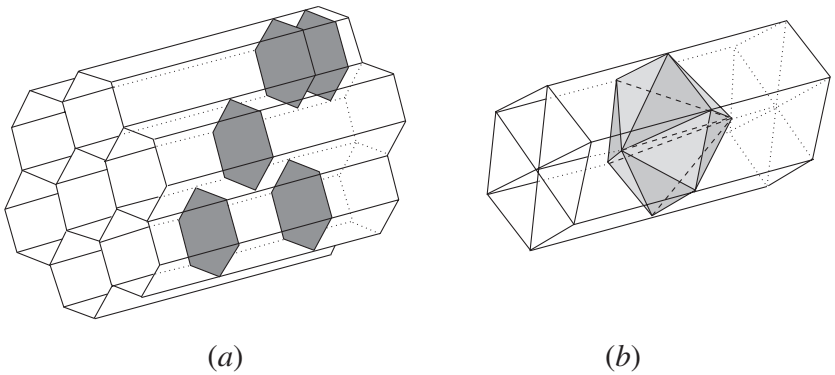

Figure 8. A sample hexagonal plaquette configuration (a). There are arbitrarily many plaquettes in each tube. Neighbouring plaquettes cannot cross each other, neither within the same tube, nor between adjacent tubes. Such configurations are dual to tetrahedral complexes, made of tetrahedra filling triangular tubes dual to the hexagonal ones. We have represented an elementary diamond-shaped building block (b) dual to a plaquette of (a), and made of six tetrahedra sharing an edge.

hexagonal section, and their array forms the two-dimensional hexagonal lattice. The plaquettes are filled hexagons orthogonal to the tubes and with the same section. A configuration is characterized by an arbitrary arrangement of such plaquettes in the tubes, where we take into account the relative ordering of the plaquettes with respect to one-another. In practice, a given plaquette only sees its nearest neighbours within the same tube and those in the six adjacent tubes, through their edges. For definiteness we attach a weight t per plaquette and consider only a finite array of tubes with transverse size $T_1 \times T_2$ and with a bulky shape. With this definition, we generate three-dimensional objects with two (time-like) regular directions and one (space-like) random one.

As in the case of triangulations where the edges are dual to pairs of triangles forming lozenges, the above hexagonal plaquettes are dual to a diamond-shaped dodecahedral volume made of six tetrahedra glued around a common edge, as shown in figure 8(b). The role formerly played by triangles is now played by tetrahedra: these live inside tubes with triangular section (dual to the original hexagonal tubes). Each such triangular tube is tessellated by tetrahedra of three possible kinds: each tetrahedron has one vertex on each edge of the tube, and the three kinds correspond to the three possible positions of the fourth vertex on one of the three edges of the tube[3]. Therefore exactly one edge of the tube contains one (space-like) edge of the tetrahedron. This edge is also common to the five other tetrahedra which together with the above form a diamond-shaped building block. All tetrahedra in a tube are glued along their triangular faces to two others in the same tube and two others in the two adjacent tubes sharing the abovementioned space-like edge.

It is interesting to view our tetrahedral complexes as a random version of some regular lattice, in the same way as the Lorentzian triangulations are deformations of the triangular lattice. To construct a regular lattice, we simply need to fill the triangular tubes with tetrahedra in a regular way, say by taking a succession of tetrahedra of the first, second, third, first, etc kinds along each tube. The other choice of chirality (first, third, second, first, etc) is completely equivalent. The resulting lattice is nothing but a FCC lattice (see figure 9). Indeed, the latter can be viewed as a regular arrangement of octahedra completed by

[3] Note that this straightforwardly generalizes the $(1+1)$D situation, where the triangles in each slice are of two kinds: those pointing up and those pointing down.

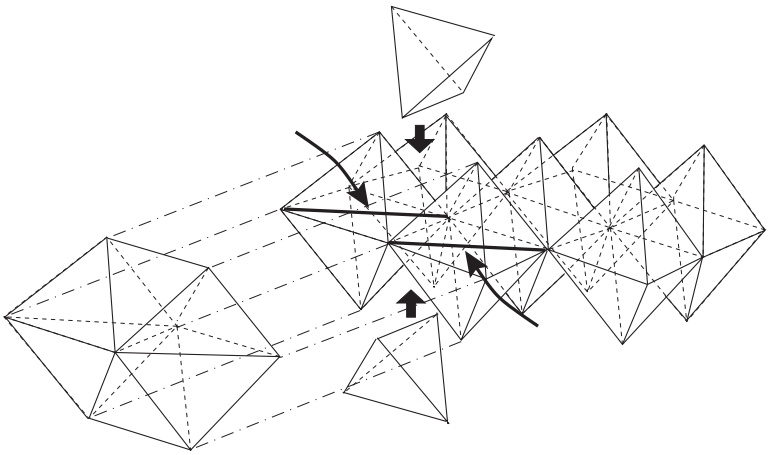

Figure 9. The regular tetrahedral complex is nothing but the FCC lattice, made of octahedra supplemented by tetrahedra as shown. To obtain only tetrahedra, we simply add a diagonal edge inside all octahedra as indicated. This allows us to decompose each octahedron into four tetrahedra. The building block of our model is composed of six tetrahedra, two from the original FCC lattice, sharing one edge, and two from each decomposed adjacent octahedron.

tetrahedra. Each octahedron can be decomposed into four tetrahedra by adding a diagonal edge (see figure 9). One possible elementary cell is obtained by first considering two original tetrahedra of the FCC lattice sharing one edge, and then by completing them by the four adjacent tetrahedra (sharing the same edge), two from each neighbouring octahedron. These six tetrahedra form the diamond-shaped building block of our model. The two choices of chirality correspond to the two possible choices of diagonal edge added inside the octahedra. In the dual plaquette language, the FCC lattice corresponds to the following regular arrangement of plaquettes: we decompose the (triangular) lattice of hexagonal tubes into three sublattices denoted, say 1, 2, 3, such that no two adjacent tubes belong to the same sublattice. Plaquettes are then arranged in equidistant successive parallel planes in such a way that plaquettes in successive planes cover the three sublattices 1, 2, 3, 1, ... alternately.

The restriction of any given tetrahedral complex to a plane generated by the longitudinal direction of the tubes and one of the three directions of the triangular lattice section of the tubes is nothing but a particular (1 + 1)D Lorentzian triangulation (see figure 10). We may therefore view the configurations of our model as the time evolution of such triangulations in successive parallel planes (with a total of T_2 plane slices), each of which extends over a fixed time lapse T_1 as shown in figure 10. The constant time lines for the Lorentzian triangulations in two successive planes are shifted by half a period of the triangular lattice of tubes: indeed, these are nothing but edges of the same triangular tube. Each triangle in a given plane is linked to a vertex of the triangulation of the next plane, belonging to the same tube. These 'face-to-vertex' tetrahedra clearly coexist with 'vertex-to-face' ones, but also with 'edge-to-edge' ones, namely with exactly one edge in each plane (one space-like and one time-like), and only time-like triangular faces.

The dual picture allows for a better understanding of the tetrahedral complex between two consecutive planes [5]. Indeed, the dual configurations of the triangulations in the lower and upper planes may be represented as in figure 11 in dashed and solid lines on the same picture, with their time lines shifted by a half-period. The three types of vertices (solid trivalent, dashed

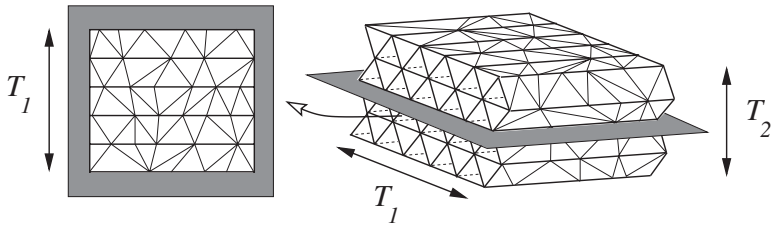

Figure 10. The horizontal section of a sample (1 + 2)D tetrahedral complex with vertical size T_2 and horizontal size T_1 is a (1 + 1)D Lorentzian triangulation over a time lapse T_1.

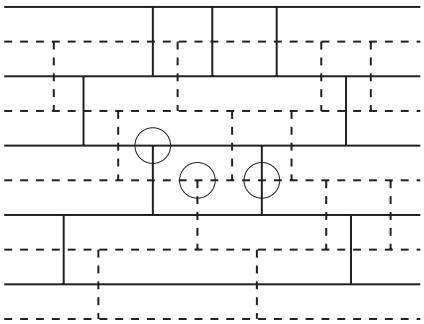

Figure 11. The dual configurations of two consecutive plane sections of a sample (1 + 2)D Lorentzian tetrahedral complex. The lower (resp. upper) configuration is represented by dashed (resp. solid) lines. The constant time lines of the two configurations are shifted by half a period. We have encircled the three types of vertices of the resulting mixed graph, in one-to-one correspondence with the three types of tetrahedra filling the slice between the two planes (see text).

trivalent and mixed tetravalent) of the resulting mixed graph are in one-to-one correspondence with the three types of tetrahedra (face-to-vertex, vertex-to-face and edge-to-edge) in the slice between the two planes.

3.2. Equivalence with hard hexagons and critical behaviour

We now wish to evaluate the partition function $Z_{\mathcal{D}}(t)$ for the Lorentzian tetrahedral complexes in the plaquette formulation inside hexagonal tubes with a total section made of a compact connected domain $\mathcal{D}$ of the hexagonal lattice. For each plaquette configuration, we define a left projection obtained by letting the leftmost plaquettes slide along the tubes all the way to their left end. The projections thus obtained are in one-to-one correspondence with configurations of hard hexagons on the two-dimensional domain $\mathcal{D}$. By hard hexagons, we mean that if a hexagon of $\mathcal{D}$ is occupied, then its immediate neighbours must be empty[4]. Repeating the arguments of section 2.1, we arrive at the following inversion formula:

$$Z_{\mathcal{D}}(t) = \frac{1}{Z^{hh}_{\mathcal{D}}(-t)} \tag{3.1}$$

[4] In the standard picture, the hardness constraint is implemented by a weaker *no-overlap* constraint for slightly larger hexagons, obtained from our hexagonal plaquettes by rotating them by $\pi/6$ and dilating them by $\sqrt{3}$. These larger hexagons are also the projections of our diamond-shaped building blocks. The two ways of implementing the hardness constraint are clearly equivalent.

where we have denoted by $Z^{hh}_{\mathcal{D}}(z)$ the partition function of the hard-hexagon model on the domain $\mathcal{D}$ with an activity z per occupied hexagon. We also have the more general formulae generalizing (2.7):

$$Z^{(C)}_{\mathcal{D}}(t) = \frac{Z^{hh}_{\mathcal{D}\backslash C}(-t)}{Z^{hh}_{\mathcal{D}}(-t)} \tag{3.2}$$

where $Z^{(C)}_{\mathcal{D}}(t)$ is the partition function for the configurations with left projection $C \subset \mathcal{D}$ and with the weight of the projection removed, while $Z^{hh}_{\mathcal{D}\backslash C}(z)$ is the hard-hexagon partition function on the domain $\mathcal{D}\backslash C$, i.e. the set of hexagonal tubes in $\mathcal{D}$ with no common edge with hexagons of C. The latter quantities (3.2) have a well-defined thermodynamic limit, obtained by keeping C fixed, and letting the domain $\mathcal{D}$ become infinite. In particular, if C is reduced to a single plaquette C_0, the quantity $Z^{(C_0)}_{\mathcal{D}}(t)$ tends to the thermodynamic density of occupied hexagons $\rho_{hh}(z = -t)$ of the hard-hexagon model. Note that this partition function $Z^{(C_0)}_{\mathcal{D}}(t)$ is the generating function of the number N_V of tetrahedral complexes with V plaquettes (i.e. tetrahedral complexes with volume V if we assign a unit volume to the diamond-shaped building block) and a single projection C_0. Note that the constraint that the projection be reduced to a single plaquette amounts to generalized 'staircase' boundary conditions.

We may now use Baxter's exact solution of the hard-hexagon model [7] to obtain the critical behaviour of $Z^{(C_0)}_{\mathcal{D}}(t)$. The hard hexagon model is known to have two critical singularities at positive and negative values of z. The singularity of our problem occurs at the negative value $z_c = \left(\frac{1-\sqrt{5}}{2}\right)^5 = \frac{11-5\sqrt{5}}{2}$ of z (corresponding to a positive $t_c = -z_c$), where the model is known to belong to the universality class of the Lee–Yang edge singularity [13, 14], itself described by a conformal field theory of central charge $c = -22/5$ [15]. The thermodynamic partition function per hexagon $\kappa_{hh}(z)$ behaves as $z \to z_c$ as

$$\kappa_{hh}(z) = \kappa_0 + \kappa_1 (z - z_c)^{\frac{5}{6}} + \mathrm{O}(z - z_c) \tag{3.3}$$

corresponding to the critical exponent $\alpha = 2 - 5/6 = 7/6$, and we also have

$$\rho_{hh}(z) = \frac{\mathrm{d}}{\mathrm{d}z}\mathrm{Log}\,\kappa_{hh}(z) \sim \frac{5}{6}\frac{\kappa_1}{\kappa_0}(z - z_c)^{-\frac{1}{6}}. \tag{3.4}$$

From this result, we immediately deduce that $Z^{(C_0)}_{\mathcal{D}}(t) \sim (t_c - t)^{-1/6}$, therefore the number N_V of tetrahedral complexes with V plaquettes and a single projection behaves for large V as

$$N_V \sim \ \mathrm{const}\frac{\left(\frac{11+5\sqrt{5}}{2}\right)^V}{V^{\frac{5}{6}}}. \tag{3.5}$$

Returning to the case of a finite but large domain $\mathcal{D}$ with area T_1T_2, we may write the partition function $Z_{\mathcal{D}}(t)$ at leading order in T_1T_2 as

$$Z_{\mathcal{D}}(t) \sim \frac{1}{\kappa_{hh}(-t)^{T_1T_2}} \sim \kappa_0^{-T_1T_2} \times \left(1 + \frac{\kappa_1}{\kappa_0}(t_c - t)^{\frac{5}{6}}\right)^{-T_1T_2}. \tag{3.6}$$

Letting the time lapses T_i scale like $T_i = \frac{\tau_i}{a}$, a a small parameter, we see that we must approach the critical point as

$$t = t_c(1 - a^{\frac{12}{5}}\Lambda) \tag{3.7}$$

where Λ is the renormalized fugacity per tetrahedron, conjugated to the renormalized volume $\mathcal{V} = Va^{12/5}$. We deduce that for large T_i

$$V \sim (T_1T_2)^{\frac{6}{5}} \tag{3.8}$$

hence the fractal dimension of the (1+2)D Lorentzian tetrahedral complexes is $d_F = 12/5$. In other words, the transverse area T_1T_2 explored by the tetrahedral complexes with V plaquettes scales like $T_1T_2 \sim V^{\frac{5}{6}}$, to be compared with the vertical length T of triangulations with A lozenges scaling like $T \sim A^{\frac{1}{2}}$.

4. Relation with directed-site lattice animals

It was shown by Dhar in [9] that $(d+1)$-dimensional problems of DSAE were related to d-dimensional nearest neighbour exclusion models. The latter include the hard-dimer model (in $d=1$ dimension) and the hard-hexagon model (in $d=2$ dimensions), respectively related to DSAE on the simple square ($d+1=2$) and simple cubic ($d+1=3$) lattices. More precisely, the generating functions of DSAE were expressed as the density of occupation of the corresponding exclusion models, which in turn reduce precisely in the hard-dimer and hard-hexagon cases to the ratios yielding $Z_T^{C_0}(t)$ and $Z_{\mathcal{D}}^{C_0}(t)$ (see equations (2.7) and (3.2)). This strongly suggests the existence of a direct connection between semi-random Lorentzian lattices and directed-site lattice animals. In this section we will indeed establish an equivalence between the two problems. As an outcome, this will give an alternative derivation of the results of [9] in a more direct way. In the following, we will focus for simplicity on the cases of (1+1)D Lorentzian triangulations and (1 + 2)D Lorentzian tetrahedral complexes.

4.1. From Lorentzian triangulations to square lattice directed animals

Let us start with the set of configurations of vertical edges of an arbitrary Lorentzian triangulation, with a fixed left projection C made of hard dimers all occupying even time slices. For each such configuration we first construct its skeleton, obtained as follows. We first decompose the edge configuration into blocks made of consecutive edges within the same time slice that are not separated by edges from neighbouring slices (see figure 12(a)). Squeezing each block into a single edge, we arrive at the skeleton of the configuration, itself a particular edge configuration with projection C, with no two consecutive edges within the same slice, as illustrated in figure 12(b). Summing over all weighted configurations sharing the same skeleton simply amounts to assigning an effective fugacity $x = t/(1-t)$ for each edge of the skeleton. Indeed, x is nothing but the sum over all block sizes $n = 1, 2, \ldots$ with a weight t^n. We may now arrange the edges of the skeleton by representing its successive left projections along regularly spaced vertical lines numbered 1, 2, 3, ... (see figure 12(b)). Noting that successive projections alternate between odd and even positions for all the edges, we see that they now lie on a regular square lattice (tilted by 45°). Moreover, the position of the edges satisfy the directed lattice animal constraint that a site on the vertical line i can be occupied only if one of its immediate neighbours on the lattice at vertical line $i-1$ is occupied (see figure 12(c)). In conclusion, the skeletons of configurations with projection C are in one-to-one correspondence with directed lattice animals on the square lattice with the same set C as 'source'. We therefore end up with an identity between the generating function $A_C(x)$ of square lattice animals with source C and activity $x = t/(1-t)$ per occupied site and the partition function of Lorentzian triangulations with activity t per dual edge and fixed left projection C

$$A_C(x) = t^{|C|}\, Z^{(C)}(t) \qquad \text{with} \quad t = \frac{x}{1+x} \tag{4.1}$$

where we have used the thermodynamic partition function $Z^{(C)}(t) = \lim_{T\to\infty} Z_T^{(C)}(t)$, well-defined for any finite C.

The inversion relation (2.7) then allows us to write $A_C(x)$ as the density of occupation $\rho_C(z)$ of the set C in the hard-dimer model with fugacity $z = -t = -x/(1+x)$, namely

$$A_C(x) = (-1)^{|C|}(-t)^{|C|}\frac{Z^{hd}_{\mathbb{Z}\setminus C}(-t)}{Z^{hd}_{\mathbb{Z}}(-t)} = (-1)^{|C|}\rho_C(-t) \tag{4.2}$$

with $t = x/(1+x)$ as before. This coincides with the result of Dhar [9]. Our derivation using left projections is slightly more direct than that of [9], which uses an intermediate connection with

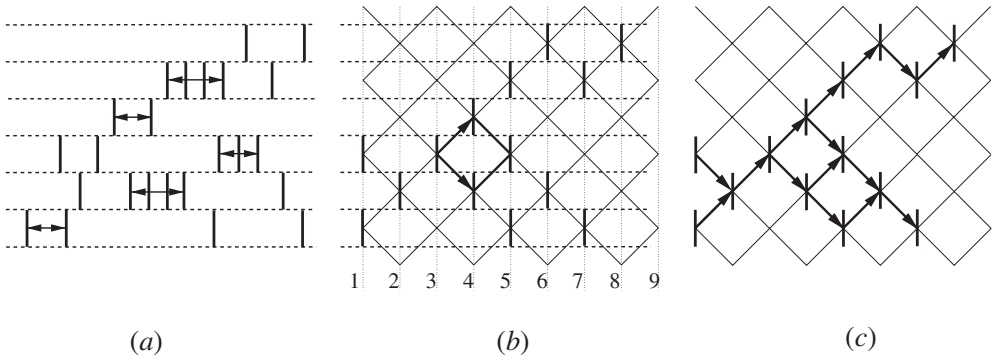

Figure 12. The equivalence between Lorentzian triangulations with a fixed left projection (with edges on even time slices) and directed-site animals on the square lattice. We first build from the configuration its skeleton obtained by squeezing all blocks into single edges (*a*). We then place the remaining edges of the skeleton onto a square lattice tilted by 45° by pushing each edge to the leftmost available position on the lattice (*b*). This is equivalent to placing the successive left projections of the skeleton onto regularly spaced vertical lines here labelled $1, 2, 3, \ldots$. We have also indicated by arrows the two successors (in the next plane) of a vertex of the square lattice. A site on line i can be occupied by an edge only if one of its two predecessors (on line $i-1$) is occupied. The occupied sites form a directed-site animal on the tilted square lattice (*c*).

a dynamical crystal-growth model and relies on the *similarity* of master equations rather than on a direct correspondence between configurations. Note also that our inversion relation (2.5) is not a simple rephrasing of the connection between directed animals and hard dimers, as it gives for instance access to the (finite size) partition function of the model of Lorentzian triangulations, which is not a density of occupation and has no direct animal interpretation. Moreover, in this section, we have artificially restricted our model to left projections with edges only in even positions, which was necessary for the animal interpretation. However we have a Lorentzian surface interpretation for all other choices of the left projection C, and a relation to hard-dimer densities as well.

4.2. From Lorentzian tetrahedral complexes to cubic lattice directed animals

The aforementioned construction generalizes nicely to the case of Lorentzian tetrahedral complexes, which are in one-to-one correspondence with directed-site lattice animals on the simple cubic lattice. We may repeat the above construction. We start again from a plaquette configuration with fixed projection C made only of plaquettes lying on one of the three triangular sublattices[5] numbered 1, 2, 3 of the triangular lattice formed by the centres of the tubes. The skeleton of the plaquette configuration is obtained again by first decomposing it into blocks of successive plaquettes within the same tube, and shrinking each of these blocks into a single plaquette. Again, the partition function of the original configurations with fixed projection C and that of the skeletons with projection C are identified by assigning an effective fugacity $x = t/(1-t)$ to the plaquettes of the skeletons. The plaquettes of the skeleton are then placed at the vertices of a simple cubic lattice by taking successive partial projections as follows. We start from the left projection C whose plaquettes lie on the sublattice, say 1, and place them on a first section plane numbered 1. The left projection of the rest of the skeleton has plaquettes now lying on the sublattices 2, 3 only. We pick the partial projection

[5] The triangular lattice is naturally decomposed into three triangular sublattices, such that no two sites of the same sublattice are adjacent.

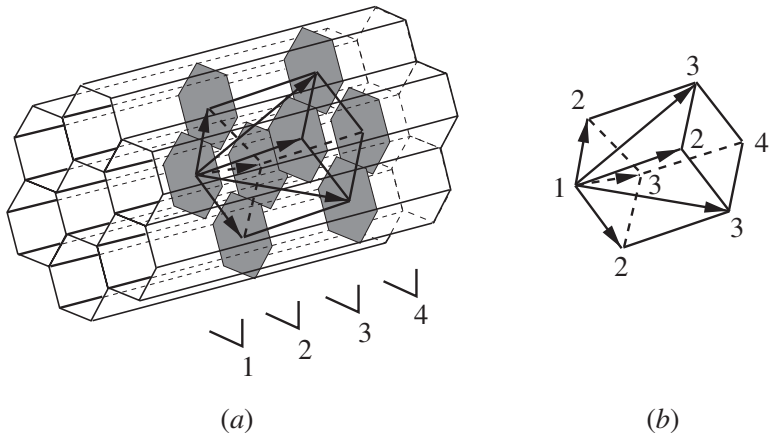

Figure 13. The possible positions (a) for plaquettes in successive partial projections of the skeletons. Plaquettes in planes $1, 2, 3, 4\ldots$ lie in the sublattices $1, 2, 3, 1\ldots$. The positions form a simple cubic lattice whose cell (b) is represented together with the label of the corresponding [111] crystalline planes. The arrows in both pictures indicate the six immediate successors (in the planes 2 and 3) of a vertex of the plane 1. For a given skeleton, only parts of the available positions are filled by plaquettes. A position of the cubic lattice can be occupied by a plaquette of a skeleton only if one of its six predecessors is occupied too.

made of the plaquettes of this projection belonging to the sublattice 2, and place them on a second plane, numbered 2, parallel to number 1, and distant by $1/\sqrt{2}$. Note that this partial projection might be empty. We then continue by considering the rest of the skeleton, whose left projection is now made of plaquettes on sublattices 3 or 1, out of which we retain those on sublattice 3, etc. Note that no two consecutive partial projection planes can be empty. The parallel partial projection planes $1, 2, 3\ldots$ are nothing but the successive [111] crystalline planes of the simple cubic lattice (see figures 13(a), (b)). The skeleton may now be interpreted as a configuration where the vertices of the simple cubic lattice may be occupied (or not) by plaquettes, with the directed-site animal constraint that a vertex in plane j may be occupied only if one of its preceding first or second nearest neighbours (respectively in planes $j-1$ and $j-2$) is occupied. This allows us to identify the generating function for DSAE on the simple cubic lattice with a fixed source C and an activity x per occupied site with the partition function of (1 + 2)D Lorentzian tetrahedral complexes with left projection C and a weight $t = x/(1+x)$ per diamond-shaped building block (i.e. $t^{\frac{1}{6}}$ per tetrahedron).

This in turn allows us to recover the relation between DSAE on the simple cubic lattice and the hard-hexagon model in two dimensions [9], in a slightly more direct manner.

5. Transfer matrices and integrability

In reference [6] it was shown that the existence of a transfer matrix formulation of pure Lorentzian triangulations was instrumental for deriving an effective one-dimensional (Calogero) Hamiltonian for the corresponding continuum scaling limit. It turns out that all the models introduced so far also have a more involved but similar transfer matrix formulation in terms of the original Lorentzian surfaces. In this section, we first show how to construct these transfer matrices, using, in particular, our inversion formula. We then show how these matrices can be regarded as particular points of integrable families of commuting matrices.

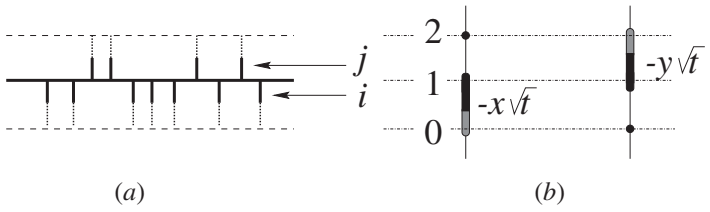

Figure 14. The transfer matrix of Lorentzian triangulations (a) connecting i lower half-edges to j upper ones across a given time line. The corresponding (non-empty) hard-dimer configurations (b) and their respective weights.

5.1. Transfer matrices for Lorentzian surfaces

Let us first recall the form of the (infinite) transfer matrix for Lorentzian triangulations. This matrix $T(t)$ transfers a row of half-edges across a time line into another row of half-edges (see figure 14(a)). A state is simply characterized by the number i (resp. j) of lower (resp. upper) half-edges, and the matrix element simply counts the number $\binom{i+j}{i}$ of ways of arranging these half-edges along the time line, together with a weight $\sqrt{t}$ per half-edge. Another way of obtaining this matrix $T(t)$ consists in computing its generating function $\Theta_1(x, y|t) = \sum_{i,j\geqslant 0} x^i y^j T(t)_{i,j}$ by use of our inversion formula (2.5), namely by expressing it as the inverse of the partition function of hard dimers on $[0, 2]$, with weights $-\sqrt{t}x$ (resp. $-\sqrt{t}y$) per dimer in the slice[6] 0 (resp. 1) (see figure 14(b)):

$$\Theta_1(x, y|t) = \frac{1}{(1 \quad \mathrm{i}y)\begin{pmatrix} 1 & \mathrm{i}\sqrt{t} \\ \mathrm{i}\sqrt{t} & 0 \end{pmatrix}\begin{pmatrix} 1 \\ \mathrm{i}x \end{pmatrix}} = \frac{1}{1-\sqrt{t}(x+y)} = \sum_{i,j\geqslant 0}\binom{i+j}{i} t^{\frac{i+j}{2}} x^i y^j. \quad (5.1)$$

Note that we have used a symmetrized version of the transfer matrix for hard dimers on the line, differing from that of (2.10) by a simple conjugation. The factors of i ensure that the dimers get the correct negative weight. This is appropriate to account for the fact that we count only half of the edge weight for the half-edges. With this definition, we have a similar formula for the Tth power of $T(t)$ generated by $\Theta_T(x, y|t)$, namely

$$\Theta_T(x, y|t) = \frac{1}{(1 \quad \mathrm{i}y)\begin{pmatrix} 1 & \mathrm{i}\sqrt{t} \\ \mathrm{i}\sqrt{t} & 0 \end{pmatrix}^T\begin{pmatrix} 1 \\ \mathrm{i}x \end{pmatrix}} \quad (5.2)$$

corresponding to the inverse of the partition function of hard dimers on $[0, T + 1]$ with a weight $-t$ per dimer on the slices $1, 2, \ldots, T - 1$ and weights $-\sqrt{t}x$ (resp. $-\sqrt{t}y$) in the slice 0 (resp. T). This quantity is simply related to the loop–loop propagator (2.22) by $\Theta_T(x, y|t) = G_{T+1}(x/\sqrt{t}, y/\sqrt{t}|t)$.

Let us now turn to the model of Lorentzian surfaces made of $2(k + 1)$-gons defined in section 2.3. To get a nice row-to-row transfer matrix $T_k(t)$, we must distinguish between the possible states in which a given half-edge can be according to its relative positioning along the full edge of size k it belongs to (see figure 15(a)). Let i_r (resp. j_r) denote the total numbers of lower (resp. upper) half-edges occupying the position $r = 1, 2, \ldots, k$ along the edges of length k they belong to. The corresponding transfer matrix elements read

$$T_k(t)_{i_1,\ldots,i_k;j_1,\ldots,j_k} = t^{\frac{1}{2k}\sum_{r=1}^k (i_r+j_r)}\binom{j_1 + \sum_{r=1}^k i_r}{j_1}\prod_{r=1}^{k-1}\delta_{j_{r+1},i_r} \quad (5.3)$$

[6] We denote by m the slice $[m, m + 1]$.

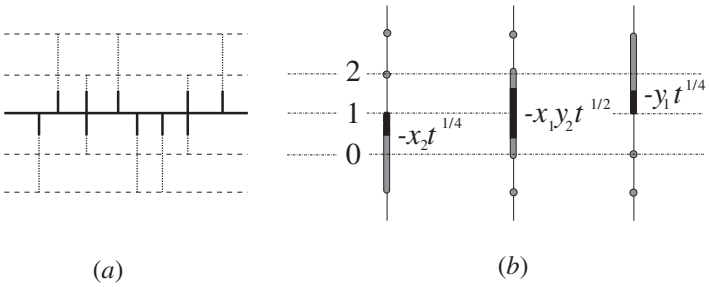

Figure 15. The transfer matrix of Lorentzian surfaces made of time-like hexagons i.e. with dual edges of fixed length $k = 2$ (*a*) connecting lower and upper half-edges across a given time line. The lower and upper half-edges each come in two types according to their position (1 or 2) along the full edge. The corresponding (non-empty) hard-trimer configurations (*b*) and their respective weights.

expressing that a half-edge in position r transfers into one in position $r+1$ for $r = 1, \ldots, k-1$ whereas one must choose the position of the j_1 *new* upper half-edges w.r.t. all the other previously existing ones, with a weight $t^{\frac{1}{2k}}$ per half-edge. Note that for $k > 1$ this transfer matrix is no longer symmetric. As before, we use the inversion formula (2.16) to write the free boundary partition function $\Theta_T^{(k)}(x_1, \ldots, x_k; y_1, \ldots, y_k|t)$ over a time lapse T as the inverse of the partition function of hard $(k+1)$-mers on $[0, T+1]$ possibly cut on the time extremities, with a weight $-t$ per $(k+1)$-mer visiting the slices $1, 2, \ldots, T-1$, and a weight $-x_r t^{\frac{2k-2r+1}{2k}}$ (resp. $-y_r t^{\frac{2r-1}{2k}}$) for a $(k+1)$-mer cut in position r in the slice 0 (resp. T), for $T \geqslant k$. When $T < k$, we must pay attention to $(k+1)$-mers that are cut at both extremities: these receive a weight $-x_r y_{T+r} t^{\frac{T}{k}}$, $r = 1, 2, \ldots, k-T$ (see figure 15(*b*)). This finally leads to

$$\begin{aligned}
&\Theta_T^{(k)}(x_1, \ldots, x_k; y_1, \ldots, y_k|t) = \frac{1}{w_k^t(y)\big(\mathcal{T}_k(t)\big)^T v_k(x)} \\
&\text{with} \quad w_k^t(y) = (\,1 \quad \alpha^{2k-1} y_1 \quad \alpha^{2k-3} y_2 \quad \cdots \quad \alpha^3 y_{k-1} \quad \alpha y_k\,) \\
&\qquad\quad v_k^t(x) = (\,1 \quad \alpha x_1 \quad \alpha^3 x_2 \quad \cdots \quad \alpha^{2k-3} x_{k-1} \quad \alpha^{2k-1} x_k\,) \\
&\mathcal{T}_k(t) = \begin{pmatrix}
1 & 0 & 0 & \cdots & 0 & \alpha t^{\frac{1}{2k}} \\
\alpha t^{\frac{1}{2k}} & 0 & 0 & \cdots & 0 & 0 \\
0 & \alpha^2 t^{\frac{1}{k}} & 0 & \cdots & 0 & 0 \\
0 & 0 & \alpha^2 t^{\frac{1}{k}} & \cdots & 0 & 0 \\
\vdots & \vdots & \vdots & \ddots & \vdots & \vdots \\
0 & 0 & 0 & \cdots & \alpha^2 t^{\frac{1}{k}} & 0
\end{pmatrix}
\end{aligned} \tag{5.4}$$

where we have set $\alpha = \mathrm{e}^{\frac{\mathrm{i}\pi}{2k}}$. The states on which $\mathcal{T}_k(t)$ acts can be understood as being, respectively, the vacuum, the first (lowest) elementary segment of the $(k+1)$-mer, the second, third, ..., kth one. As before, the phases in (5.4) ensure that all multimers (including the cut ones) have a minus sign in front of the fugacity. Note also the explicit 'up–down' symmetry of $\mathcal{T}_k(t)$ implemented by the symmetric matrix $\mathcal{R}_{i,j} = \delta_{j,k+1-i}$ for $i, j \geqslant 1$ and $\mathcal{R}_{0,j} = \delta_{j,0}$, namely that the matrix $\mathcal{R}\mathcal{T}_k(t)$ is symmetric and that $\mathcal{R}v_k(x) = w_k(x)$. This translates into the symmetry of $\Theta_T^{(k)}$ under the interchange of $x_r \leftrightarrow y_{k+1-r}$, $r = 1, 2, \ldots, k$. A preliminary remark is in order: if we take the formula (5.4) for $T = 0$, we get

$$\Theta_0^{(k)}(x_1, \ldots, x_k; y_1, \ldots, y_k|t) = \frac{1}{1 - \sum_{r=1}^k x_r y_r} = \sum_{i_1, \ldots, i_k \geqslant 0} \frac{(\Sigma i_r)!}{\Pi i_r!} \prod_{r=1}^k (x_r y_r)^{i_r} \tag{5.5}$$

which generates the diagonal matrix P with diagonal entries $P_{i_1,\ldots,i_k} = \frac{(\Sigma i_r)!}{\Pi i_r!}$ rather than just the identity. More generally, $\Theta_T^{(k)}$ is the generating function for $\big(T_k(t)\big)^T P$, where the boundary operator P corresponds to a preliminary ordering of the half-edges of the initial state over which $T_k(t)$ acts. Note that the action of $T_k(t)$ automatically orders the final state. In particular, for $T = 1$ the result (5.4) reduces to

$$\Theta_1^{(k)}(x_1,\ldots,x_k;\, y_1,\ldots,y_k|t) = \frac{1}{1 - t^{\frac{1}{2k}}(x_k + y_1) - t^{\frac{1}{k}}(x_1y_2 + x_2y_3 + \cdots + x_{k-1}y_k)}$$
$$= \sum_{i_1,\ldots,i_k,j_1\geqslant 0} t^{\frac{j_1+i_k+2\Sigma_{1\leqslant r\leqslant k-1} i_r}{2k}} (x_1y_2)^{i_1}\ldots(x_{k-1}y_k)^{i_{k-1}} x_k^{i_k} y_1^{j_1} \frac{(j_1+\Sigma_{1\leqslant r\leqslant k} i_r)!}{j_1!i_1!i_2!\ldots i_k!} \tag{5.6}$$

which is nothing but the generating function of $T_k(t)P$, with $T_k(t)$ as in (5.3). The up–down symmetry is recovered by noting that $RT_k(t)R = P^{-1}T_k(t)^t P$, where R is the matrix with entries $R_{i_1,\ldots,i_k;\,j_1,\ldots,j_k} = \prod_{r=1}^k \delta_{j_r,i_{k+1-r}}$ corresponding to the interchange $x_r \leftrightarrow x_{k+1-r}$, while the transposition expresses the interchange of x_r and y_r.

More generally, the above construction can be generalized to the hard-multimer models of section 2.2, leading to an explicit transfer matrix formulation of the corresponding generalized Lorentzian surfaces. Details are presented in the appendix. Finally, let us mention that the above extends straightforwardly to higher dimensions. In the case of (1 + 2)D Lorentzian tetrahedral complexes, for instance, we may define a 'plane-to-plane' transfer matrix acting in the second time direction (T_2, see figure 10) and transferring from a (1 + 1)D Lorentzian triangulation to the one above (see figure 11). The generating function for this transfer matrix (multiplied by a diagonal ordering operator P as before) is expressed as the inverse of a decorated partition function for hard hexagons via our inversion formula. The latter is itself the generating function for the matrix elements of the row-to-row transfer matrix for hard hexagons [7].

5.2. Integrability and the inversion relation

In reference [4] it was observed that the model of pure Lorentzian triangulations was a point ($a = 1$) along an integrable family of models including both triangles and squares (with two time-like and two space-like edges), with weights $a\sqrt{t}$ per triangle and $u = t(1 - a^2)$ per square. The corresponding surfaces are generated in the dual picture by means of a row-to-row transfer matrix $T(t, a)$ whose element $T(t, a)_{i,j}$ corresponds to the transfer from i lower vertical edges to j upper ones across a time line, $i, j \geqslant 0$. It was shown that the transfer matrices $T(t, a)$ and $T(t', a')$ commute provided

$$\frac{1 - t(1 - a^2)}{a\sqrt{t}} = \frac{1 - t'(1 - a'^2)}{a'\sqrt{t'}}. \tag{5.7}$$

In our language this model with triangles and squares corresponds to having $2(k + 1)$-gons of arbitrary size $k = 1, 2, 3, \ldots$ made of the piling up of $(k-1)$ squares across k consecutive time slices, and terminated by two triangles on the top and bottom of the pile. These objects come with a weight $t_k = a^2tu^{k-1}$, $k = 1, 2, 3, \ldots$. We immediately deduce from our general inversion formula that the partition function $\mu(t, a)$ for these surfaces with left staircase boundary conditions and with semi-infinite time range $[0, \infty)$ satisfies equation (2.20)

$$\mu = 1 + \sum_{k=1}^{\infty} a^2tu^{k-1}\mu^{k+1} \Rightarrow t\mu^2 = (1 + u)\mu - 1. \tag{5.8}$$

Upon rescaling $\tilde{\mu} = (1+u)\mu$ and $\tilde{t} = t/(1+u)^2$ we end up with the same equation as that of the pure Lorentzian triangulation case $a = 1$ ($u = 0$). As a non-trivial outcome of our formulation, the integrability condition for the infinite size transfer matrices $T(t, a)$ can be deduced from a similar condition on the 2×2 transfer matrices of the corresponding hard-multimer models. Let us write the generating function $\Theta_2(x, y|a, t, a', t') = \sum_{i,j\geqslant 0} x^i y^j (T(t', a')T(t, a))_{i,j}$ of the product $T(t', a')T(t, a)$ as the inverse of a multimer partition function on [0, 2] with weights $-a\sqrt{t}x$ (resp. $-aa'\sqrt{tt'}$ and $-a'\sqrt{t'}y$) for dimers in slice 0 (resp. 1 and 2), $-a'\sqrt{t'}ux$ (resp. $-a\sqrt{t}u'y$) for trimers covering the slices 0, 1 (resp. 1, 2) and finally $-xyuu'$ for quadrimers covering all the slices. This reads

$$\Theta_2(x, y|a, t, a', t') = \frac{1}{\begin{pmatrix} 1 & \mathrm{i}y \end{pmatrix} \begin{pmatrix} 1 & \mathrm{i}a'\sqrt{t'} \\ \mathrm{i}a'\sqrt{t'} & u' \end{pmatrix} \begin{pmatrix} 1 & \mathrm{i}a\sqrt{t} \\ \mathrm{i}a\sqrt{t} & u \end{pmatrix} \begin{pmatrix} 1 \\ \mathrm{i}x \end{pmatrix}}. \tag{5.9}$$

Similarly the generating function $\Theta_2(x, y|a', t', a, t)$ is expressed by the same formula with the two 2×2 matrices exchanged. The commutation of the original transfer matrices translates therefore into that of these two 2×2 ones. A simple calculation shows that they commute provided $(1-u)/(a\sqrt{t}) = (1-u')/(a'\sqrt{t'})$, which is precisely the integrability condition (5.7).

This suggests to look for integrable families of finite size matrices corresponding to decorated multimer models and to interpret them as integrable models of more involved Lorentzian surfaces. For simplicity, let us consider the case of symmetric $(k+1) \times (k+1)$ matrices. For illustration, we may consider a model of coloured hard dimers with a colour index $i = 1, 2, \ldots, k$, and a weight z_i for each dimer of colour i, with transfer matrix

$$\mathcal{T}_0 = \begin{pmatrix} 1 & \sqrt{z_1} & \sqrt{z_2} & \cdots & \sqrt{z_k} \\ \sqrt{z_1} & 0 & 0 & \cdots & 0 \\ \sqrt{z_2} & 0 & 0 & \cdots & 0 \\ \vdots & \vdots & \vdots & & \vdots \\ \sqrt{z_k} & 0 & 0 & \cdots & 0 \end{pmatrix}. \tag{5.10}$$

This is nothing but the original hard-dimer model with fugacity $z = z_1 + z_2 + \cdots + z_k$. However, we now want to view it as a particular point of an integrable family of transfer matrices $\mathcal{T}$, depending on $k(k+3)/2$ new parameters $\mathcal{T}_{i,j} = \mathcal{T}_{j,i}$, $i, j = 0, 1, 2, \ldots, k$ where we fix $\mathcal{T}_{0,0} = 1$. The parameters $\mathcal{T}_{0,j} = \sqrt{w_j}$, $j = 1, 2, \ldots, k$ are interpreted as new fugacities per dimer of colour j. The numbers $\mathcal{T}_{i,j}$ for $i, j \geqslant 1$ can be interpreted as follows. We first allow the dimers to pile up so as to form multicoloured multimers of length m, and we assign a weight $\sqrt{w_{i_1} w_{i_m}} \prod_{p=1}^{m-1} \mathcal{T}_{i_p, i_{p+1}}$ for each $(m+1)$-mer formed by a sequence of dimers of colours $i_1, i_2, \ldots, i_m$. To get an integrable family, we must impose that all the $\mathcal{T}$ share the same orthonormal basis of eigenvectors as $\mathcal{T}_0$ (this involves fixing a $(k-1)$-dimensional rotation acting on the kernel of $\mathcal{T}_0$). Denoting by $\psi_i^{(m)}$ the ith entry of the mth eigenvector of $\mathcal{T}_0$, and by Λ_m the corresponding mth eigenvalue of $\mathcal{T}$, for $i, m = 0, 1, 2, \ldots, k$, we have

$$\mathcal{T}_{i,j} = \sum_{m=0}^{k} \Lambda_m \psi_i^{(m)} \psi_j^{(m)} \tag{5.11}$$

where the Λ_m are free parameters satisfying the constraint

$$\mathcal{T}_{0,0} = 1 = \sum_m \Lambda_m (\psi_0^{(m)})^2. \tag{5.12}$$

This shows that the matrices $\mathcal{T}$ form generically a k-parameter family passing by the point $\mathcal{T}_0$ (with $w_i = z_i$). This also gives a parametrization of the dimer factors $\mathcal{T}_{0,i} = \sqrt{w_i} =$

$\sum_m \Lambda_m \psi_0^{(m)} \psi_i^{(m)}$ in terms of the $k+1$ eigenvalues Λ_m. Let us display the case $k=1$ for illustration. We first diagonalize the matrix $\mathcal{T}_0 = \begin{pmatrix} 1 & \mathrm{i}\sqrt{t} \\ \mathrm{i}\sqrt{t} & 0 \end{pmatrix}$ with the resulting eigenvectors:

$$\psi^{(0)\,t} = \frac{1}{\sqrt{1-q^2}}\big(1, \mathrm{i}q\big) \qquad \psi^{(1)\,t} = \frac{1}{\sqrt{1-q^2}}\big(\mathrm{i}q, -1\big) \tag{5.13}$$

where we have set $1/\sqrt{t} = q + 1/q$, and $q < 1$. The one-parameter integrable family takes the form

$$\mathcal{T}_{i,j} = (1 + \mathrm{i}q\sqrt{w})\psi_i^{(0)}\psi_j^{(0)} + (1 + \mathrm{i}\sqrt{w}/q)\psi_i^{(1)}\psi_j^{(1)} \tag{5.14}$$

where we have parametrized the eigenvalues Λ_0 and Λ_1, satisfying $\Lambda_0(\psi_0^{(0)})^2 + \Lambda_1(\psi_0^{(1)})^2 = 1$ in terms of the matrix element $\mathcal{T}_{0,1} = \sqrt{w}$. Equation (5.14) coincides with $\mathcal{T} = \begin{pmatrix} 1 & \mathrm{i}a\sqrt{t} \\ \mathrm{i}a\sqrt{t} & u \end{pmatrix}$ provided $\sqrt{w} = \mathrm{i}a\sqrt{t}$ and $u = t(1-a^2)$.

A slight generalization of the previous case allows us to include the general Lorentzian surfaces models of sections 2.2 and 2.3 in larger integrable families. As opposed to the previous case, the corresponding transfer matrix $\mathcal{T}_0$ is no longer symmetric (see for instance equation (5.4)). Still, the 'up–down' symmetry of the problem allows us to make the transfer matrix symmetric, by use of a certain involution $i \to r(i)$ of its indices, implementing the up–down reflection of the multimers, while preserving the vacuum ($r(0) = 0$). More precisely, let $\mathcal{R}$ be the matrix with entries $\mathcal{R}_{i,j} = \delta_{j,r(i)}$, then the up–down symmetry of $\mathcal{T}_0$ translates into the fact that $\mathcal{R}\mathcal{T}_0$ is symmetric. We now may look for an up–down symmetric integrable deformation $\mathcal{T}$ of $\mathcal{T}_0$, namely such that $\mathcal{R}\mathcal{T}$ is symmetric, and moreover satisfying the condition that $\mathcal{T}_{0,0} = 1$. Denoting again by $\psi_i^{(m)}$ a basis of diagonalization of $\mathcal{T}_0$, we first note that by virtue of up–down symmetry it can be normalized so as to be '$\mathcal{R}$-orthonormal', namely that $\big(\mathcal{R}\psi^{(m)}\big)^t \psi^{(p)} = \delta_{m,p}$. We still write the family $\mathcal{T}$ in a form similar to (5.11), taking into account the up–down symmetry, namely

$$\mathcal{T}_{i,j} = \sum_m \Lambda_m \psi_i^{(m)} \psi_{r(j)}^{(m)} \tag{5.15}$$

where the Λ satisfy the same constraint as before: $\mathcal{T}_{0,0} = 1 = \sum_m \Lambda_m (\psi_0^{(m)})^2$. The case of hard $(k+1)$-mers of section 2.3 is obtained by taking $\mathcal{T}_0 \equiv \mathcal{T}_k(t)$ of equation (5.4), with the same up–down symmetry matrix $\mathcal{R}_{i,j} = \delta_{j,k+1-i}$ for $i, j = 1, 2, \ldots, k$ and $\mathcal{R}_{0,j} = \delta_{j,0}$. The case of hard multimers of the appendix corresponds to taking $\mathcal{T}_0 \equiv \mathcal{T}^{(hm)}$, and the up–down symmetry matrix $\mathcal{R} = \mathcal{R}^{(hm)}$.

In conclusion, we have shown that all the 1D hard-multimer transfer matrices used in this paper are part of larger integrable families corresponding to the introduction of extra interactions between multimers. This in turn implies that all the transfer matrices for Lorentzian surfaces defined in section 2 are also part of larger integrable families allowing for the original polygonal tiles to form larger composite objects, with new weights. This extends nicely to the case of (1 + 2)D Lorentzian tetrahedral complexes as well. Indeed, as noted by Baxter [7], the hard-hexagon model is part of a larger integrable family (hard-square model with diagonal interactions). Once translated in the language of plaquettes this amounts to allowing hexagons to coexist on neighbouring sites along one of the three directions of the triangular lattice of tubes, with a new contact Boltzmann weight. The corresponding transfer matrices form via our inversion relation the desired integrable family of models, describing complexes in which the diamond-shaped building blocks can be glued together along that same direction so as to form larger straight objects of arbitrary length, with new Boltzmann weights.

6. Discussion and conclusion

In this paper, we initially investigated general models of (1+1)D Lorentzian surfaces. Viewing the pure Lorentzian triangulations as semi-random surfaces made only of time-like lozenges, we considered semi-random surfaces made of larger time-like tiles, namely obtained by piling up lozenges, thus forming $2(i+1)$-gons, $i = 1, 2, 3 \ldots$. All these models have been solved by the use of an inversion relation expressing their partition functions in terms of those of associated hard multimers in 1D. We then showed how to obtain multicritical models of these generalized Lorentzian surfaces by an appropriate fine-tuning of the activities of the various tiles. These models involve only time-like interactions, a key point for the inversion relation to 1D hard objects to hold. Indeed, this relation relies entirely on the fact that the only horizontal (space-like) coupling is through the no-crossing prescription of edges. It would be interesting however to try to build more involved inversion relations, possibly using horizontal (space direction) transfer matrices between successive vertical projections, and use them to solve models with horizontal (space-like) as well as vertical (time-like) interactions, such as the Ising model on Lorentzian surfaces.

We then generalized our construction so as to build a new higher-dimensional model of (1 + 2)D Lorentzian tetrahedral complexes, with two regular (time-like) and one random (space-like) directions. This model was solved by using a generalized higher-dimensional version of the previous inversion formula, relating it to the 2D hard-hexagon model solved by Baxter [7]. This model is the most natural extension of that of Lorentzian triangulations to higher dimension with tetrahedra playing the role of triangles. We also showed how to interpret the model as the time evolution of Lorentzian triangulations in successive layers. In this respect, we obtain a toy-model for (2 + 1)D Lorentzian gravity, where the space-like triangulations are restricted to be themselves Lorentzian. It is interesting to note that other plaquette models can be similarly constructed by considering tubes with sections forming different lattices. For instance, we may consider a model of square plaquettes with square lattice section or of triangular plaquettes with triangular lattice section. In an analogous way, the latter are, respectively, related to the hard-square and hard-triangle models in two dimensions. Unfortunately, these have not yet been solved exactly, although very precise results are known about them [16]. More importantly, when we try to interpret these as models of simplicial Lorentzian manifolds, we find that the corresponding elementary simplices (replacing the tetrahedra) become degenerate objects with pairs of vertices linked by more than one edge, that are usually discarded in simplicial gravity. For this reason we did not expand on these models. Another possible generalization is to keep hexagonal tubes and tetrahedra as elementary objects, but to form larger building blocks than the diamond-shaped dodecahedra considered so far. These larger objects are obtained by gluing several dodecahedra in the two time directions in the same way as we did for lozenges. Models based on these building blocks with, say, activities t_i for the ith type of block are still related to models of hard objects on the triangular lattice, namely with plaquettes obtained by gluing hexagonal plaquettes together, and attaching activities $z_i = -t_i$ to them. These 2D models seem not to have been considered yet (in particular, they are not identical to the so-called ABF models [17] generalizing the hard-hexagon model). Still it is very plausible that by again fine-tuning the activities t_i one should be able to reach multicritical points. It is natural to believe that these correspond to non-unitary conformal field theories with central charges $c(2, 2m-1) = 1 - 3(2m-3)^2/(2m-1)$, where the case of hard hexagons corresponds to the Lee–Yang edge singularity with $m = 3$, $c = -22/5$. The corresponding thermal dimension is known to be $h_{1,3} = (5-2m)/(2m-1)$ henceforth the singularity of the free energy has the critical exponent $2 - \alpha = 1/(1-h_{1,3}) = (2m-1)/(2(2m-3))$. The

corresponding fractal dimension of the associated multicritical Lorentzian manifolds would read $d_F = 4(2m-3)/(2m-1)$.

Let us also point out that there is an obvious natural higher-dimensional generalization of tetrahedral complexes, now built with $d+1$-simplices living in $d+1$-dimensional 'tubes' whose d-dimensional section is the regular d-dimensional generalization of the FCC lattice [18], in correspondence with a model of nearest neighbour exclusion on the vertices of that lattice.

Another direction of generalization consists in staying in low dimension e.g. in $(1+1)$D, but to introduce disorder in the form of randomly distributed activities, but constant within each tube. Indeed, the inversion relation of this paper holds as well for each realization of the disorder, with fixed tube-dependent activities. In the case of quenched disorder, where we must compute the average $\overline{\log Z}$ over all possible realizations of the disorder, we can use the inversion formula term by term in the average, to write the result as minus the quenched disorder average of the corresponding hard-object model, namely $-\overline{\log Z_h}$. Clearly, the inversion relation does not allow us to relate the two annealed disorder partition functions $\overline{Z}$ and $\overline{Z_h}$ of the two problems.

Another type of disorder consists in considering plaquette models with fixed activities but defined on tubes whose section is itself arranged into random graphs, in connection to the corresponding nearest neighbour exclusion problem on the same graphs. Again, the two quenched disorder problems are identical up to a sign.

We may also consider tubes with section arranged into an arbitrary but fixed graph. An interesting choice for such a graph is one where the nearest neighbour exclusion model has already been solved, in which case we can immediately convert the solution into that of the corresponding Lorentzian plaquette model. One such example is the infinite rooted q-valent graph known as the Bethe lattice, $q = 2, 3, \ldots$. The corresponding plaquettes are q-gons, each connected to one q-gon in the previous shell and to $q-1$ ones in the next. A simple calculation (see e.g. [16]) shows that the thermodynamic free energy of the nearest neighbour exclusion model $f_{\rm nne}(z)$ per site, with an activity z per occupied site, reads

$$f_{\rm nne}(z) = \left(1 - \frac{q}{2}\right) \mathrm{Log}\,(2 - \mu(-z)) - \frac{q}{2} \mathrm{Log}\,\mu(-z) \tag{6.1}$$

where $\mu(t)$ is the Fuss–Catalan generating function (2.24) with $k = q$, obeying the equation $z = (1-\mu(t))/\mu(t)^q$, $t = -z$. For $q \geqslant 2$, the first singularity of $f_{\rm nne}(z)$ for $z < 0$ occurs at the value $z = z_c$ such that $\mu(-z_c) = q/(q-1)$, resulting in a singularity with exponent $2 - \alpha = 1/2$, translating into a fractal dimension $d_F = 2$ for the corresponding Bethe Lorentzian surfaces.

Finally, the models considered here were shown to contain lattice animals as a subclass. Conversely, we may apply this equivalence backwards to investigate more refined properties of our semi-random lattices. In particular, directed lattice animals are known to have two distinct characteristic lengths, a longitudinal and a transversal one, each with its own scaling exponent $\nu_\parallel$ and $\nu_\perp$. While $\nu_\perp$ refers to our time correlation length exponent (with $d_F = 1/\nu_\perp$), it would be interesting to interpret the second exponent in terms of our semi-random lattices. On the other hand, the animals interpretation holds as well for models with $2(i+1)$-gons $i = 1, 2, 3 \ldots$. However the animals corresponding, for instance, to $(1+1)$D models with edges of fixed length $k \geqslant 2$ are quite unconventional, not to speak of those corresponding to the multicritical models.

After completion of this work, we became aware of reference [19] where an analogous inversion formula as that for $(1+1)$D pure Lorentzian triangulations was derived in the context of commutative monoids, and of more recent developments on lattice animals and exclusion models [20, 21].

Acknowledgments

We thank T Garel for pointing out reference [9] to us, and J-M Luck for useful discussions. We also thank D Dhar for pointing out reference [19] to us and M Bousquet-Mélou for further references.

Appendix. Transfer matrix for general multimers

Let us consider the general model of Lorentzian surfaces made of $2(i+1)$-gons $i = 1, 2, \ldots, k$ of section 2.2. It is easy to see that the corresponding transfer matrix $T^{(hm)}$ is expressed in terms of a hard-multimer one (denoted by $\mathcal{T}^{(hm)}$) through a formula similar to (5.4). The matrix $\mathcal{T}^{(hm)}$ is obtained by superposing those for fixed i (with respective transfer matrices $\mathcal{T}_i(t)$ as in (5.4)) in the following manner. It must act on the following states: the vacuum (label 0), the unique dimer (label 1), the first segment of a trimer (label 2), the second segment of a trimer (label 3), ..., the jth segment of a $(i+1)$-mer (label $I(i,j) = j + i(i-1)/2$ for $j = 1, 2, \ldots, i$), ... the kth segment of a $(k+1)$-mer (label $k(k+1)/2$). The matrix $\mathcal{T}^{(hm)}$ therefore has total size $1 + k(k+1)/2$ and its elements read

$$\begin{aligned}
&\mathcal{T}^{(hm)}_{0,0} = 1 \\
&\mathcal{T}^{(hm)}_{0,I(i,j)} = \mathcal{T}_i(t)_{0,j} && i, j \geqslant 1 \\
&\mathcal{T}^{(hm)}_{I(i,j),0} = \mathcal{T}_i(t)_{j,0} && i, j \geqslant 1 \\
&\mathcal{T}^{(hm)}_{I(i,j),I(i,m)} = \mathcal{T}_i(t)_{j,m} && i, j, m \geqslant 1 \\
&\mathcal{T}^{(hm)}_{I(i,j),I(p,m)} = 0 && \text{for} \quad i \neq p
\end{aligned} \tag{A.1}$$

where $\mathcal{T}_i(t)$ is as in (5.4). Note that this matrix is also 'up–down' symmetric in the sense that $\mathcal{R}^{(hm)}\mathcal{T}^{(hm)}$ is symmetric, where $\mathcal{R}^{(hm)}$ is the symmetric matrix with entries

$$\begin{aligned}
&\mathcal{R}^{(hm)}_{0,0} = 1 \\
&\mathcal{R}^{(hm)}_{0,I(i,j)} = \mathcal{R}^{(hm)}_{I(i,j),0} = 0 \\
&\mathcal{R}^{(hm)}_{I(i,j),I(p,m)} = \delta_{p,i}\delta_{m,i+1-j}
\end{aligned} \tag{A.2}$$

for $1 \leqslant j \leqslant i \leqslant k$. The matrix $\mathcal{T}^{(hm)}$ leads through a formula analogous to (5.4) to the generating function $\Theta^{(hm)}_T(\{x_{I(i,j)}\}; \{y_{I(p,m)}\}|t_1, \ldots, t_k)$ of $\left(T^{(hm)}\right)^T P^{(hm)}$ where the diagonal matrix $P^{(hm)}$ implements the ordering of the initial state over which $T^{(hm)}$ acts. More precisely, we have

$$\begin{aligned}
&\Theta^{(hm)}_T(\{x_{I(i,j)}\}; \{y_{I(p,m)}\}|t_1, \ldots, t_k) = \frac{1}{w^t\left(\mathcal{T}^{(hm)}\right)^T v} \\
&\text{with} \quad w_{I(i,j)} = (w_i)_j(y_{I(i,j)}) \qquad w_0 = 1 \\
&v_{I(i,j)} = (v_i)_j(x_{I(i,j)}) \qquad v_0 = 1
\end{aligned} \tag{A.3}$$

which for $T = 0$ generates the elements of the diagonal matrix $P^{(hm)}$ with diagonal entries:

$$P^{(hm)}_{\{i_{I(p,m)}\}} = \frac{(\sum i_{I(p,m)})!}{\prod i_{I(p,m)}!} \tag{A.4}$$

while the formula (A.3) leads for $T = 1$ to the transfer matrix elements

$$T^{(hm)}_{\{i_{I(p,m)}\};\{j_{I(p,m)}\}} = \prod_{p=1}^{k} \left(t^{\frac{1}{2p}\sum_{r=1}^{p}(i_{I(p,r)}+j_{I(p,r)})} \prod_{r=1}^{p-1} \delta_{j_{I(p,r+1)},i_{I(p,r)}} \right) \times \frac{\left(\sum_{p=1}^{k}(j_{I(p,1)} + \sum_{r=1}^{p} i_{I(p,r)})\right)!}{\left(\sum_{1\leqslant r\leqslant p\leqslant k} i_{I(p,r)}\right)! \prod_{p=1}^{k} j_{I(p,1)}!}. \tag{A.5}$$

For illustration, the matrix $\mathcal{T}^{(hm)}$ reads for $k = 2$:

$$\mathcal{T}^{(hm)} = \begin{pmatrix} 1 & \mathrm{i}\sqrt{t_1} & 0 & \alpha t_2^{\frac{1}{4}} \\ \mathrm{i}\sqrt{t_1} & 0 & 0 & 0 \\ \alpha t_2^{\frac{1}{4}} & 0 & 0 & 0 \\ 0 & 0 & \mathrm{i}\sqrt{t_2} & 0 \end{pmatrix} \tag{A.6}$$

where $\alpha = \mathrm{e}^{\mathrm{i}\pi/4}$. This leads to the matrices

$$\begin{aligned} P^{(hm)}_{i_1,i_2,i_3} &= \frac{(i_1+i_2+i_3)!}{i_1!i_2!i_3!} \\ T^{(hm)}_{i_1,i_2,i_3;j_1,j_2,j_3} &= t_1^{\frac{i_1+j_1}{2}} t_2^{\frac{2j_2+i_3+j_2}{4}} \delta_{j_3,i_2} \frac{(i_1+i_2+i_3+j_1+j_2)!}{(i_1+i_2+i_3)!j_1!j_2!} \end{aligned} \tag{A.7}$$

where i_1 (resp. i_2, i_3) denote the total numbers of halves of single edges (resp. halves of first, second segments of edges of length 2) in the lower part and similarly for the j in the upper part. Note that the combinatorial factor in the second line of (A.7) expresses the choice of position of the two new types of edges (of respective length 1 and 2, in numbers j_1 and j_2) w.r.t. the already existing ones.

References

[1] Di Francesco P, Ginsparg P and Zinn-Justin J 1995 2D gravity and random matrices *Phys. Rep.* **254** 1–131

[2] Ambjørn J, Durhuus B and Johnsson T 1997 *Quantum Geometry* (Cambridge: Cambridge University Press)

[3] Ambjørn J and Loll R 1998 Non-perturbative Lorentzian quantum gravity, causality and topology change *Nucl. Phys.* B **536 [FS]** 407 (hep-th/9805108)

[4] Di Francesco P, Guitter E and Kristjansen C 2000 Integrable 2D Lorentzian gravity and random walks *Nucl. Phys.* B **567 [FS]** 515 (hep-th/9907084)

[5] Ambjørn J, Jurkiewicz J and Loll R 2001 Non-perturbative 3D Lorentzian quantum gravity *Phys. Rev.* D **64** 044011 (hep-th/0011276)

[6] Di Francesco P, Guitter E and Kristjansen C 2001 Generalized Lorentzian gravity in 1 + 1D and the Calogero Hamiltonian *Nucl. Phys.* B **608[FS]** 485–526 (hep-th/0010259)

[7] Baxter R J 1980 Hard hexagons: exact solution *J. Phys. A: Math. Gen.* **13** L61–70
Baxter R J and Tsang S K 1980 Entropy of hard hexagons *J. Phys. A: Math. Gen.* **13** 1023–30
see also Baxter R J 1984 *Exactly Solved Models in Statistical Mechanics* (London: Academic)

[8] Cardy J 1982 Directed lattice animals and the Lee–Yang edge singularity *J. Phys. A: Math. Gen.* **15** L593–5

[9] Dhar D 1982 Equivalence of two-dimensional directed-site animal problem to Baxter's hard-square lattice gas model *Phys. Rev. Lett.* **49** 959–62
Dhar D 1982 Exact solution of a directed-site animals-enumeration problem in three dimensions *Phys. Rev. Lett.* **51** 853–6

[10] Bisch D and Jones V 1997 Algebras associated to intermediate subfactors *Inv. Math.* **128** 89

[11] Lang W 2000 On generalizations of the Stirling number triangles *J. Integer Seqs.* **3** #00.2.4 and references therein

[12] Bateman H 1953 *Higher Transcendental Functions* vol 3 (New York: McGraw-Hill)

[13] Kurze D and Fisher M 1979 Yang–Lee edge singularities at high temperatures *Phys. Rev.* B **20** 2785

[14] Di Francesco P, Saleur H and Zuber J-B 1988 Generalized Coulomb gas formalism for two-dimensional critical models based on $SU(2)$ coset construction *Nucl. Phys.* B **300 [FS]** 393–432

[15] Cardy J 1985 Conformal invariance and the Yang–Lee edge singularity in two dimensions *Phys. Rev. Lett.* **54** 1354–6

[16] Baxter R J 1999 Planar lattice gases with nearest-neighbour exclusion *Ann. Combin.* **3** 191–203 (cond-mat/9811264)

[17] Andrews G, Baxter R and Forrester P 1984 Eight vertex SOS model and generalized Rogers–Ramanujan type identities *J. Stat. Phys.* **35** 193–266

[18] Bowick M, Di Francesco P, Golinelli O and Guitter E 1995 Three-dimensional folding of the triangular lattice *Nucl. Phys.* B **450 [FS]** 463–94 (cond-mat/9502063)

[19] Viennot G 1986 Heaps of pieces I: basic definitions and combinatorial lemmas *Combinatoire Énumérative (Lecture Notes in Math. vol 1234)* ed G Labelle and P Leroux pp 321–46

[20] Bétréma J and Penaud J 1994 Modèles avec particules dures, animaux dirigés, et séries en variables partiellement commutatives *Labri Report* webpage http://dept-info.labri.u-bordeaux.fr/ betrema

[21] Bousquet-Mélou M and Rechnitzer A 2000 Lattice animals and heaps of dimers *Labri Preprint* webpage http://dept-info.labri.u-bordeaux.fr/ bousquet/publis.html